Exploiting *Pseudomonas syringae* Type 3 secretion to study effector contribution to disease in spinach

Melanie Mendel[1,2], Xander C. L. Zuijdgeest[1,3], Femke van den Berg[1], Leroy van der Meer[1], Joyce Elberse[2], Petros Skiadas[4], Michael F Seidl[4], Guido Van den Ackerveken[2], Ronnie de Jonge[1,5*]

[1]Plant-Microbe Interactions, Department of Biology, Faculty of Science, Utrecht University, 3584 CH, Utrecht, The Netherlands

[2]Translational Plant Biology, Department of Biology, Faculty of Science, Utrecht University, 3584 CH, Utrecht, The Netherlands

[3] Current address: Centre for Plant Molecular Biology (ZMBP), University of Tübingen, 72076 Tübingen, Germany

[4] Theoretical Biology and Bioinformatics, Department of Biology, Faculty of Science, 3584 CH, Utrecht, The Netherlands

[5]AI Technology For Life, Department of Information and Computing Sciences, Science for Life, Utrecht University, 3584 CC, Utrecht, The Netherlands

* corresponding author: Ronnie de Jonge, r.dejonge@uu.nl

Keywords: spinach, *Pseudomonas syringae*, effectors, effector screening, plant immunity

Funding: TopSector TKI Tuinbouw & Uitgangsmaterialen Grant Number: LWV19284, Enza Zaden Research & Development B.V. (NL), Pop Vriend Seeds (subsidiary of KWS Vegetables BV) (NL), Rijk Zwaan Breeding B.V. (NL), and Syngenta (NL).

22 ## Abstract

23 Intensive cultivation practices of spinach create favourable conditions for the emergence and rapid
24 evolution of pathogens, causing substantial economic damage. Research on host-pathogen interactions
25 and host immunity in various leafy greens benefits from advanced biotechnological tools. The absence
26 of specialised tools for spinach, however, constrains our understanding of spinach immunity. Here, we
27 explored the potential of Type III Secretion System (T3SS)-mediated delivery to study the activity of
28 pathogen effectors in spinach. We identified the *Pseudomonas syringae* pv*. tomato* DC3000 (DC3000)
29 polymutant D36E, which lacks 36 known T3SS effectors (T3Es), as a promising T3SS-dependent effector
30 delivery system in spinach. Unlike DC3000, which causes visual disease symptoms on spinach, D36E did
31 not induce visible disease symptoms. Using D36E effector delivery, we screened 28 known DC3000 T3Es
32 individually on spinach for effects on disease symptom development, bacterial proliferation reflecting
33 bacterial virulence, and ROS bursts as a proxy for early immune responses. All three assays identified
34 T3Es AvrE1 and HopM1 as crucial determinants of DC3000-like infection on spinach. Additionally, we
35 observed that the T3E HopAD1 strongly suppressed ROS production in spinach. We present the first
36 experimental evidence of plant pathogen effector activities in spinach. By establishing the D36E-effector
37 delivery system in spinach, we pave the way for high-throughput effector studies on spinach. This system
38 provides a critical link between genomics-based effector predictions in spinach pathogens and
39 experimental validation, which is a crucial step for knowledge-driven resistance breeding in non-model
40 crops like spinach.

41

42 ## Introduction

43 As consumers increasingly opt for healthier dietary alternatives, spinach has seen a remarkable rise in
44 its economic significance (Kandel et al., 2019). To meet the increasing demand, growers cultivate spinach
45 at high intensity, providing favourable conditions for the outbreak and rapid evolution of pathogens. For
46 instance, the pathogenic oomycete *Peronospora effusa* (*Pe*) poses a major threat to global spinach
47 production because it primarily infects spinach leaves, causing downy mildew disease making the
48 product unsalable and thus leading to substantial economic damage (Ribera et al., 2020). Other
49 agronomically relevant spinach pathogens are *Albugo occidentalis, Colletotrichum dematium,*
50 *Pythium spp.* and viruses like cucumber mosaic virus (CMV) (Kandel et al., 2019; Ribera et al., 2020). To
51 mitigate the impact of rapidly evolving pathogens on spinach production, targeted improvement of crop
52 resistance is crucial. However, in contrast to other leafy greens like lettuce, we currently lack
53 biotechnological tools to study immunity in spinach, thereby hampering our ability to rapidly identify
54 novel disease resistance traits.

55 Our current understanding of the spinach immune system is limited and largely relies on comparative
56 genome analysis and analysis of gene expression profiles in the context of disease resistance. For
57 example, transcriptomic analysis comparing *Pe*-susceptible and *Pe*-resistant spinach cultivars showed
58 that known defence-related genes like *PR-1* and diverse types of immune receptor genes are
59 upregulated in resistant spinach cultivars (Kandel et al., 2020). This suggests that, certain components
60 of the plant immune system are likely conserved in spinach. The first layer of plant immune system
61 detects intruders through characteristic molecular patterns. The recognition of patterns by extracellular
62 receptors activates a generic immune response called Pattern-Triggered Immunity (PTI) that is
63 characterized, for example, by the rapid production of reactive oxygen species (ROS) (Ngou et al., 2022;

64 Zhang et al., 2023a). In spinach, the receptor-like kinase *FERONIA* is upregulated in *Pe*-resistant cultivars
65 and it has been hypothesized to be involved in ROS production (Kandel et al., 2020).

66 Successful pathogens subvert the first layer of the plant immune system with the help of small, secreted
67 proteins called effectors (Wang et al., 2022). In contrast, resistant plants can detect the presence of
68 effectors and re-initiate and intensify their immune responses upon the recognition of effectors leading
69 to effector-triggered immunity (ETI) (Ngou et al., 2021; Yuan et al., 2021). ETI typically involves
70 programmed cell death, known as the hypersensitive response (HR), which is thought to prevent the
71 spread of pathogens (Jones and Dangl, 2006). ETI is typically initiated by immune receptors such as the
72 receptor-like kinases (RLKs) and nucleotide-binding leucine-rich repeat receptors (NLRs) (Ngou et al.,
73 2022). The spinach genome encodes several hundred NLRs (Xu et al., 2017; Hulse-Kemp et al., 2021),
74 and some of these have already been implicated in spinach resistance to *Pe*. Fine mapping of the *RPF2*
75 (Resistance to *Peronospora farinosa* 2) resistance locus against *Pe* race 16, e.g., revealed a ~600 Kbp
76 region on spinach chromosome 3 that comprise multiple candidate resistance genes including NLRs
77 (Bhattarai et al., 2021; Gao et al., 2022). Although spinach is a dicot plant, its immune receptor repertoire
78 resembles more that of monocots, e.g in their NLR composition (Hulse-Kemp et al., 2021). This suggests
79 that while some aspects of the spinach immune system are likely conserved, notable differences to
80 related plant species are to be expected (Liu et al., 2021). This underscores the importance of dedicated
81 exploration to understand the distinct functions of the spinach immune system.

82 Currently, we know little about the specific processes that occur during spinach-pathogen interaction,
83 including the activity and targets of pathogen effectors. Only recently, genomic resources for spinach
84 and its pathogens, became available, importantly *Pe*, which alone was predicted to harbour a repertoire
85 of >300 effectors (Hulse-Kemp et al., 2021; Fletcher et al., 2022). To date, no specific pathogen effector

86 has been identified to be recognized by spinach (Cai et al., 2021), while such knowledge would benefit
87 breeding efforts for resistance in spinach. The large number of predicted effectors encoded by spinach
88 pathogens necessitates the development of methods to screen these effectors for their contribution to
89 disease or their recognition by spinach immune receptors. Typically, *Agrobacterium*-mediated transient
90 expression assays are used to screen for effector recognition and investigate effector function in crops
91 (Lu et al., 2016; Pelgrom et al., 2019). However, attempts to use this system to study effector function
92 in spinach were unsuccessful, possibly due to inefficient transient transformation, low expression levels,
93 or significant background noise (Neilen, 2020). Recent reports on improving *Agrobacterium*-mediated
94 transient expression in spinach involved substantial fine-tuning of individual protein expression levels,
95 making it less suitable for high-throughput effector screening (Zhang et al., 2023b). Alternatives, such as
96 biolistic methods, nanoparticles, chemical transformations, fusion peptides, and the bacterial Type 3
97 Secretion System (T3SS), can be used to deliver proteins and predicted effector candidates into plants,
98 but these approaches have not yet been explored in spinach (Rustgi et al., 2022).

99 Here, we evaluated the potential of T3SS-mediated delivery as a method for studying pathogen effectors
100 in spinach. The T3SS, a molecular syringe, is essential for the delivery of bacterial effectors into the host
101 cell (O'Malley and Anderson 2021). T3SS mutants display reduced virulence, underscoring the
102 importance of T3SS-delivered effectors (T3Es) in establishing disease (Yuan and He 1996). Using the
103 effectorless *Pseudomonas syringae* pv. *tomato* DC3000 polymutant D36E, we show that in the absence
104 of T3Es, D36E survives in spinach leaves while causing no significant disease symptoms. To verify if D36E
105 can deliver effectors in spinach, we reintroduced 28 known DC3000 T3Es into D36E and evaluated their
106 contribution to disease symptom development, bacterial proliferation, and ROS burst alterations, an
107 early marker of plant immunity. We demonstrate the effects of several of these effectors on these

108 phenotypes in spinach, supporting previous evidence that they target conserved components of plant
109 immunity and physiology.

110 ## Results

111 ### Identification of *Pseudomonas* strain D36E as a candidate for T3SS-dependent effector delivery in
112 spinach.

113 To study effectors in spinach, we first sought to identify a T3SS-encoding bacterial strain that is suited
114 for the delivery of effectors through the T3SS into spinach. As initial indicator of a bacterium's suitability
115 for T3SS-dependent effector delivery, we tested for the absence of disease symptoms and the
116 bacterium's ability to sustain a population when inoculated into spinach leaves (Figure 1). We tested
117 multiple *Pseudomonas* strains which were previously employed to deliver effectors in other hosts, i.e.:
118 1) the Effector-to-Host-Analyser strain (EtHAn), a non-pathogenic *Pseudomonas fluorescence* (*Pf*-0)
119 strain, genetically engineered to express a T3SS and which has been employed in multiple plants across
120 several studies (Thomas et al., 2009; Krasileva et al., 2011; Upadhyaya et al., 2013); 2) the wildtype
121 *Pseudomonas syringae* pv*. tomato* DC3000 (DC3000) strain, a natural pathogen of tomato and which
122 was used to study effectors in other plants (Buell et al., 2003; Fabro et al., 2011); 3) multiple DC3000
123 mutants with reduced effector arsenals, i.e., the DC3000$^{\Delta CEL}$(Δ*CEL*) mutant that lacks a conserved
124 effector locus, the nearly effectorless DC3000^{D28E} (D28E) polymutant, and the effectorless polymutant
125 DC3000^{D36E} (D36E) (Alfano et al., 2000; Cunnac et al., 2011; Wei et al., 2015); and 4) a *Pseudomonas*
126 *syringae* pv*. phaseolicola* (*Psp*) strain, which is a natural pathogen of bean that displayed promising
127 results in preliminary work on spinach (Arnold et al., 2011). Lastly, we include a fourth DC3000 mutant,
128 the T3SS mutant DC3000$^{\Delta hrcC}$ (Δ*hrcC*). This mutant cannot assemble a functional T3SS and therefore not
129 deliver T3Es at all (Yuan and He, 1996).

130 We syringe-infiltrated the first true leaves of 2.5-3-week-old spinach with *Pseudomonas* bacteria at
131 optical densities at 600 nm (OD_{600}) equal to 0.2, 0.4 and 0.6. Between 6 days post inoculation (dpi) and

132 7 dpi, we visually assessed disease symptoms confirming that Δ*hrcC* and *Psp* did not cause visible disease
133 symptoms. The three strains EtHAn, DC3000 and Δ*CEL* caused strong and consistent disease symptoms
134 at all tested concentrations, while D28E and D36E showed mild plant symptoms (Figure 1A). At the
135 highest titre, D28E infiltration resulted in mild chlorosis. To estimate the survival or proliferation of
136 bacterial populations in spinach, we next measured bacterial titres in spinach as colony-forming units
137 (CFUs) at 0 dpi and 2 dpi (Figure 1B). The Δ*hrcC* and D36E strains showed significantly reduced bacterial
138 titres at 2 dpi compared to 0 dpi of around 1.5-2 orders of magnitude. *Psp*, like Δ*hrcC,* at OD_{600} 0.2,
139 showed reduced bacterial titres between 0 dpi and 2 dpi, but at the higher titres (OD_{600} equal to 0.4 and
140 0.6) *Psp* resulted in sustained bacterial titres at 2 dpi around the 0 dpi levels which might suggest that
141 native *Psp* effectors aid the stabilization of titres. EtHAn, DC3000 and Δ*CEL*, all of which exhibited disease
142 symptoms, proliferated in spinach between 0 dpi and 2 dpi, increasing titres around 1.5-2 orders of
143 magnitude. In contrast, D28E and D36E behaved similar to Δ*hrcC*, stabilising at titres 1-1.5 orders of
144 magnitude lower at 2 dpi compared to 0 dpi. We conclude that the effectorless D36E polymutant is a
145 suitable strain for effector delivery into spinach because it induced no disease symptoms, yet encodes a
146 functional T3SS. To assess whether D36E sustains a population in spinach after 2 dpi, we next evaluated
147 its titres in leaves for a prolonged period of 5 days (Figure S1). We found that D36E titres remain stable
148 after 1 dpi, similar to DC3000, indicating that in the absence of visible plant responses D36E is able to
149 survive in spinach for at least 5 days (Figure S1). These findings prompted us to further investigate the
150 use of D36E as an effector delivery system in spinach.

151 ### AvrE1 and HopM1 are key contributors to DC3000-like disease symptoms in spinach

152 Since infiltration of wildtype DC3000 bacteria causes disease symptoms in spinach while D36E bacteria
153 did not (Figure 1), we hypothesised that the development of disease symptoms following DC3000

154 infiltration in spinach results from the delivery and successive disease-promoting functions of some of
155 its effectors. To test this hypothesis and assess D36E's suitability as an effector delivery system, we
156 reintroduced 28 DC3000 effectors one-by-one into D36E, thereby creating a library of D36E strains with
157 single DC3000 effectors and evaluated their effect on disease symptom development and bacterial
158 proliferation in spinach. Upon infiltration, we observed a variety of disease symptoms ranging from no
159 symptoms or mild chlorosis (D36E-like; disease score 0) to strong necrosis (DC3000-like; disease score 4)
160 (Figure 2; S2).

161 Of the 28 tested single effector D36E strains, 18 did not show clear disease symptoms and were not
162 significantly different compared to D36E. The remaining 10 yielded a diversity of disease symptoms and
163 strains carrying *AvrE1* or *HopM1* stood out as infiltration with these strains consistently yielded strong
164 disease symptoms in >80% of infiltrated spots (Figure 2). Notably, these symptoms were similar to those
165 obtained by DC3000 infiltration. Similarly, D36E carrying *HopAM1*, *HopF2*, or *HopN1* yielded clear disease
166 symptoms in >65% of infiltrated spots. Infiltration of D36E carrying *HopF2* frequently also led to strong
167 chlorosis, at times combined with necrotic lesions (disease score >1 in 75%). These symptoms were
168 markedly different from symptoms observed after infiltration with DC3000, or D36E carrying *AvrE1* or
169 *HopM1*. D36E carrying *HopAM1* and *HopN1* also resulted in the development of necrotic lesions distinct
170 from DC3000, e.g., necrosis induced by HopN1 was patchy and less intense compared to DC3000.
171 Infiltration of D36E carrying *AvrPtoB*, *HopAD1*, *HopAO1*, *HopR1* and *HopU1* elevated the frequency of
172 disease symptoms, although clear disease symptoms (>1) were found to be less consistent in this group,
173 only manifesting in 27%-47% of infiltrated spots.

174 ## AvrE1, HopM1 and HopU1 significantly affect bacterial proliferation in spinach

175 Virulence of bacterial pathogens, defined as the ability of a pathogen to successfully establish a
176 population in the host, can be quantified by assessing proliferation in the host (Fabro et al., 2011). One
177 measurable way to evaluate bacterial proliferation, is by assessing bacterial titres as previously described
178 (Liu et al., 2015). Therefore, we next examined the contribution of the 28 single effectors to D36E
179 proliferation in spinach, and identified three that significantly affected D36E titres in spinach (Figure 3).
180 Among these three, *AvrE1* and *HopM1* were notable for significantly increasing D36E titres. Conversely,
181 D36E carrying *HopU1* resulted in a lower titre. D36E bacteria carrying *HopAD1*, *HopAO1*, or *HopF2*
182 exhibited a tendency towards higher titres, while D36E carrying *HopAA-1*, *HopN1* and *HopX1* showed a
183 trend towards reduced titres. The remaining 18 D36E strains did not significantly differ in their titres
184 from the D36E control, suggesting that these have limited impact on D36E proliferation in spinach.

185 Surprisingly, among the effectors that did not significantly alter D36E proliferation are those that induced
186 the strongest disease symptoms, i.e., *HopN1*, *HopAM1* and *HopF2* (Figure 2, 3). Thus, there appears to
187 be a correlation between effector-driven symptom development and bacterial proliferation for some of
188 the effectors, most notably AvrE1 and HopM1. Although, such correlation is not general and likely related
189 to the corresponding effector function.

190 ## AvrE1, HopM1 and HopAD1 lower early spinach ROS bursts

191 Bursts of reactive oxygen species (ROS bursts) are an early immune response against plant colonisation
192 by pathogens (Ngou et al., 2022). Consequently, successful pathogens are able to suppress ROS bursts
193 (Jwa and Hwang, 2017). To gain insight into the functional role of effectors in managing early immune
194 responses in spinach, we established a ROS burst assay in spinach in combination with the D36E effector
195 delivery system. First, we developed a D36E-compatible ROS burst assay in spinach based on described

196 *Nicotiana benthamiana* methodology (Johanndrees et al., 2022). In short, we first set out to identify
197 potent ROS burst elicitors in spinach and next developed a suitable assay, including appropriate controls
198 and concentrations, for infiltration of bacteria. To find potent elicitors, we tested previously described
199 ROS burst elicitors chitin (Sánchez-Vallet et al., 2015), the 22-amino-acid flg22 peptide (Mersmann et al.,
200 2010), the 24-amino-acid nlp24 peptide of downy mildew Nep1-like protein 3 (Oome et al., 2014) and
201 elicitor mixes of heat-lysed D36E cells (Wei et al., 2015) and heat-lysed *Peronospora effusa Race 1* (*Pe1*)
202 spores (Klein et al., 2020; Skiadas et al., 2022) (details in Table S5) for their ability to elicit a ROS burst in
203 spinach leaf discs. We found that chitin, heat-lysed D36E cells and heat-lysed *Pe1* spores triggered
204 significant ROS bursts in spinach (Figure S3), and we picked heat-lysed D36E as the MAMP as it showed
205 the strongest ROS bursts.

206 Next, we established controls for D36E-compatible ROS assays. To this end, we compared ROS
207 production in leaf discs from leaves that were pre-infiltrated with either D36E or a mock solution one
208 day before conducting the ROS assay. We found that pre-infiltration with D36E bacteria does not change
209 base ROS levels or ROS bursts compared to mock-infiltration (Figure S4). Hence, we further utilized D36E-
210 infiltrated, mock-treated samples (D36E/MQ) as negative controls for ROS assays, and D36E-infiltrated,
211 MAMP-treated samples (D36E/MAMPs) as positive controls. We observed that pre-infiltration with
212 DC3000 lowered the MAMP-induced ROS bursts (Figure S5), and, furthermore, we found that infiltration
213 with DC3000 bacteria at OD_{600} equal to 0.4 or 1.0 led to a significant reduction in ROS bursts compared
214 to DC3000 pre-infiltration with OD_{600} equal to 0.04 or D36E (OD_{600} equal to 0.4), which did not
215 significantly alter ROS bursts (Figure S5). Together, this indicates that infiltration with the intermediate
216 titre at 0.4 is most suited for the detection of ROS burst-suppressive effectors.

217 Subsequently, we screened our single effector library in D36E for ROS burst suppression using this assay.
218 To compensate for the relatively high variation between ROS assays we focussed on relative changes in
219 relative light units (RLUs) as this parameter appears to be most robust for capturing ROS bursts in
220 spinach. Relative changes in RLUs were normalised by the D36E/MQ negative control in each assay to
221 limit the impact of batch effects, applied a $\log_2$ transformation, and quantified the obtained ROS burst
222 by calculating the area under the curve (AUC) for each sample. Finally, to facilitate interpretation, we
223 scaled the results by the D36E/MAMPs positive control (Figure 4).

224 Analysis of the ROS bursts showed that D36E bacteria carrying *AvrE1*, *HopAD1* or *HopM1* significantly
225 suppressed the ROS burst in comparison to D36E bacteria (Figure 4). *HopAD1*, especially, reduced ROS
226 bursts back to levels of the negative control D36E/MQ, which is even below DC3000 wildtype ROS burst
227 suppression. D36E carrying *HopF2*, *HopAO1*, or *HopN1* showed a trend towards reducing ROS bursts,
228 while *AvrPtoB*, *HopU1* and *HopY1* showed a trend towards increasing the ROS burst. As before, the
229 majority of effectors in D36E did not alter the ROS burst significantly.

230 AvrE1 and HopM1 alone can largely restore DC3000-like characteristics on spinach

231 We observed a notable increase in *Pseudomonas* proliferation alongside heightened disease symptom
232 development in our initial experiments to identify *Pseudomonas* isolates suitable for T3SS-dependent
233 delivery of effector proteins in spinach (Figure 1), as well as during our single effector screening
234 experiments (Figure 2,3). A similar trend appeared to exist between ROS burst suppression and bacterial
235 proliferation (Figure 3,4), which was also reported before (Jwa and Hwang, 2017) (Figure 4). To delve
236 deeper into these relationships, we systematically compared the diverse phenotypic outcomes
237 associated with each of the DC3000 effectors expressed in D36E. To facilitate a comparative analysis, we
238 standardized the different quantitative phenotypes using Z-scaling and performed hierarchical clustering

239 (Figure 5A). Additionally, we performed linear regression analysis between the phenotypic results and
240 plotted results for the respective comparisons (Figure 5B).

241 We unveiled five distinct clusters of single effector lines (I-V), each characterized by unique features
242 (Figure 5A). Cluster I consists of the DC3000 wildtype, and D36E bacteria carrying either *HopM1* or *AvrE1*
243 corroborating earlier observations that these effectors can largely restore DC3000-like effects in spinach
244 for the assessed phenotypes (Figure 4A,5A). Cluster II represents a single D36E effector strain: HopAD1.
245 D36E carrying *HopAD1* strongly lowered ROS bursts while neither affecting proliferation nor disease
246 symptoms (Figure 2,3,4,5A), suggesting that ROS burst suppression is not sufficient to restore D36E
247 proliferation and development of disease in spinach. Cluster III comprises D36E bacteria carrying *HopR1*,
248 *HopAM1*, *HopN1*, *HopF2* and *HopAO1* (Figure 5A). These bacteria enhanced disease symptom
249 development, with a trend towards lowering ROS bursts but had little impact on bacterial proliferation
250 (Figure 2,3,4). Cluster IV comprised D36E bacteria carrying *AvrPtoB* and *HopU1* (Figure 5A). These
251 effectors reduced bacterial proliferation, significantly only in the case of *HopU1* (Figure 3), and exhibited
252 a trend towards enhancing the ROS burst and disease symptom development (Figure 2, 4). This
253 combination of reduced proliferation and the presence of visible disease symptoms challenged our initial
254 hypothesis of a positive correlation between proliferation and disease symptoms. Potentially, these
255 effectors might trigger activation of the immune system which would be consistent with reduced
256 proliferation, heightened ROS bursts and possibly immune-related symptoms such as programmed cell
257 death. The largest cluster, cluster V, comprises the remaining 18 D36E effector lines which did not
258 significantly alter any of the quantified phenotypes in spinach (Figure 5A).

259 Altogether, the systematic analysis suggests that there is a modest correlation between effector
260 contributions to disease symptom development, proliferation, and ROS burst suppression, that is,

261 however, carried primarily by just two effectors, i.e. AvrE1 and HopM1. Still, also among the other
262 effectors, we observe a trend that contribution to disease symptom development likely also affects
263 proliferation and/or ROS burst suppression.

264 ## Discussion

265 To further advance knowledge-driven resistance breeding in spinach, it is essential to develop simple
266 and scalable *in planta* validation of candidate effectors. Here, we describe the characterization of the
267 DC3000 polymutant D36E bacterium (D36E) as an effector delivery system in spinach. This system
268 allowed us to identify DC3000 effectors with a significant impact on disease symptom development,
269 bacterial proliferation, and ROS bursts. By screening 28 DC3000 effectors in D36E, we identified AvrE1
270 and HopM1 as key drivers for DC3000-like performance of D36E on spinach. We also identified HopAD1
271 as a powerful suppressor of ROS bursts in spinach. Moreover, we found that the effectors HopAM1,
272 HopF2, HopN1 and HopR1 contributed to disease symptoms without significantly affecting D36E
273 proliferation. To our knowledge, this is the first report of functional *in planta* effector screens in the
274 non-model crop spinach.

275 In our analysis, expression of *AvrE1* and *HopM1* in D36E resulted in comparable phenotypes on spinach.
276 Functional redundancy among these two effectors was extensively described on model plants including
277 DC3000's natural host, tomato, but also *Nicotiana benthamiana* and *Arabidopsis thaliana* (DebRoy et al.,
278 2004; Badel et al., 2006; Cunnac et al., 2011). In DC3000, they are encoded alongside each other at the
279 conserved effector locus (*CEL*) which is widely distributed among plant-infecting bacteria of the genus
280 *Pseudomonas* (Baltrus et al., 2011). Both effectors contribute to the creation of an aqueous micro-
281 environment on host plants which is crucial for successful *Pseudomonas* infection (Roussin-Léveillée et
282 al., 2022). In spinach, we observed water-soaked lesions, symptomatic for the establishment of an
283 aqueous micro-environment, upon inoculation with D36E bacteria carrying *AvrE1* or *HopM1* at around
284 2 dpi. This suggests that their virulence targets are conserved in spinach.

285 On the molecular level, AvrE1 and HopM1 are distinct, belonging to different molecular families. AvrE1
286 belongs to a broadly conserved AvrE1/DspA/E/HopR1 superfamily of effectors (Kvitko et al., 2009;
287 Baltrus et al., 2011), while HopM1 is part of a less conserved effector family (Baltrus et al., 2011;
288 Jayaraman et al., 2020). AvrE1 is the best characterized effector of its superfamily, recently
289 demonstrated to induce water-soaked lesions by forming a pore-forming beta barrel, thereby creating a
290 permeable membrane channel (Nomura et al., 2023). The pore-forming function appears not to be
291 shared by HopM1, which does not exhibit the distinct beta barrel structure or other prominent molecular
292 features (Nomura et al., 2023). In spinach, we observed that AvrE1, more than HopM1, could induce
293 DC3000-like symptoms by D36E (Figure 4), likely via its pore-forming function. To establish the aqueous
294 micro-environment, AvrE1 also affects abscisic acid (ABA)-dependent regulation of stomatal opening and
295 concomitantly, transpiration (Roussin-Léveillée et al., 2022). Independent of a functional pore-
296 formation, AvrE1-family effector WtsE was linked to ABA regulation via an interaction with protein
297 phosphatase 2A (PP2A), a known player in ABA signalling (Jin et al., 2016). This interaction involved an
298 *N*-terminal fragment of WtsE (residues 1- 964), outside of the pore-forming beta-barrel region. Strikingly,
299 *Ha*RxL23, an effector encoded by the oomycete *Hyaloperonospora arabidopsidis*, the causal agent of
300 downy mildew disease on Arabidopsis, displays structural similarity to the *N*-terminus of AvrE1, outside
301 of the pore-forming beta barrel (Deb et al., 2018) In *Arabidopsis*, HaRxL23 was shown to partially
302 complement an *avrE1* deletion mutant of DC3000, suggesting convergent evolution of AvrE1 and
303 oomycete effectors towards similar host processes (Deb et al., 2018).

304 HopM1, like AvrE1, was implicated in creating water-soaked lesions to enhance virulence in *Arabidopsis*
305 (Xin et al., 2016), which aligns with phenotypes we observed in spinach. HopM1 was shown to target the
306 proteasome, a central point of regulation in plant immunity (Üstün et al., 2016). HopM1 enhances

307 AtMIN7 proteasome-dependent degradation consequently interfering with vesicle transport in
308 *Arabidopsis* (Nomura et al., 2006; Xin et al., 2016). In addition, HopM1 destabilises a range of other
309 proteins in a proteasome-dependent manner that include, e.g., 14-3-3 proteins like GRF8/TFT1 (Lozano-
310 Durán et al., 2014). HopM1 was shown to reduce PAMP-triggered ROS bursts, similar to chemical
311 destabilisation of 14-3-3 proteins or a targeted silencing of GRF8/TFT1, suggesting that HopM1 targets
312 14-3-3 proteins to supress early immune responses like ROS bursts (Lozano-Durán et al., 2014). We
313 observed that infiltration of spinach leaves with D36E carrying *HopM1* significantly suppressed the ROS
314 burst, suggesting that the interference with 14-3-3 proteins might be conserved (Figure 4).

315 Infiltration of spinach leaves with D36E bacteria carrying *HopAD1* led to a strong suppression of the ROS
316 burst and occasionally led to the development of mild necrosis (Figure 2, 4). Compared to AvrE1/HopM1,
317 less information is available for HopAD1, as it was initially dismissed as a non-functional effector (Chang
318 et al., 2005). Wei and colleagues, however, also described its potential to suppress the ROS burst and
319 trigger cell death in *N. benthamiana* (Wei et al., 2015). When the effector AvrPtoB is present, like in the
320 case of DC3000, HopAD1's immunogenic activities are masked in *N. benthamiana* leading to the earlier
321 dismissal of this effector (Wei et al., 2015). The nearly effector-less DC3000 mutant D28E, does not
322 encode *AvrPtoB*, which enabled Wei and colleagues to reveal its function (Wei et al., 2015). While in
323 spinach and in *N. benthamiana*, infiltration by D36E bacteria carrying *HopAD1* yielded strong suppression
324 of the ROS burst, only in *N. benthamiana*, infiltration at high titres also resulted in consistent cell death
325 symptoms (Wei, Zhang et al. 2018, Figure 2, 4). Also in *N. benthamiana*, cell-death did not necessarily
326 lead to altered virulence, mimicking our findings in spinach (Wei, Zhang et al. 2018, Figure 2, Figure 5).
327 Thus, we describe the observed symptoms as an indication of development of disease to clearly
328 distinguish it from the hypersensitive response, which is an immune response. Overall, we suggest that

329 the suppression of the ROS burst is a primary function of HopAD1, which by itself appears to be
330 insufficient to promote bacterial proliferation. Despite the identification of HopAD1's immunogenic
331 activity, the molecular mechanisms underlying its ability to suppress the ROS burst while leaving
332 bacterial proliferation unaffected in spinach remain elusive.

333 In nature, effectors often act synergistically and display redundancy. For instance, our findings reveal
334 that the Δ*CEL* mutant, characterized by the absence of *AvrE1*, *HopM1*, *HopN1* and *HopAA-1* (Alfano et
335 al., 2000; Wei and Collmer, 2018), induced robust disease symptoms and exhibited proliferation similar
336 to the wildtype at 2 dpi on spinach (Figure 1). This finding contrasts with our observations of single
337 effectors, wherein only *AvrE1* and *HopM1* could significantly enhance proliferation of D36E bacteria on
338 spinach. However, its DC3000-like virulence underscores the importance of synergistic effector action in
339 nature. The combined influence of the remaining effectors in the Δ*CEL* mutant appears to compensate
340 for the absence of *AvrE1* and *HopM1* in spinach, emphasizing the intricate collaboration among effectors
341 in shaping the overall pathogenic response. Evidence for genetic interactions between DC3000 effectors
342 was found before in *N. benthamiana*, wherein HopAD1-dependent disease symptoms are suppressed by
343 AvrPtoB, and HopI1 suppressed cell death elicited by AvrE1, HopM1, HopR1, HopQ1-1 and HopAM1 (Wei
344 et al., 2015).

345 Looking ahead, we believe that the D36E delivery system can be harnessed for characterising spinach
346 pathogen effectors. Compared to native spinach-pathogens like *Pe*, the D36E effector delivery provides
347 a simplified system for studying effectors in their native host to characterize individual effectors.
348 Whether the D36E system allows the identification of effectors recognised by the spinach immune
349 system remains an open question. Our study is limited to native DC3000 effectors, none of them

350 exhibiting the combination of reduced bacterial proliferation and visual cell-death symptoms which we
351 would expect for the detection of an effector by the plants' immune system (Wei et al., 2018).

352 In conclusion, we introduce the first high-throughput method for functional effector studies in spinach.
353 Our results, applied to deliver bacterial DC3000 effectors, unveil potential strategies of spinach
354 pathogens by targeting proteins associated with ABA signalling, stomatal aperture, 14-3-3 proteins, and
355 various phosphatases, such as PP2A. Our established T3SS-based effector delivery method serves as a
356 bridge, alleviating a significant bottleneck in knowledge-driven resistance breeding for spinach and other
357 non-model crops.

358

359 Figures

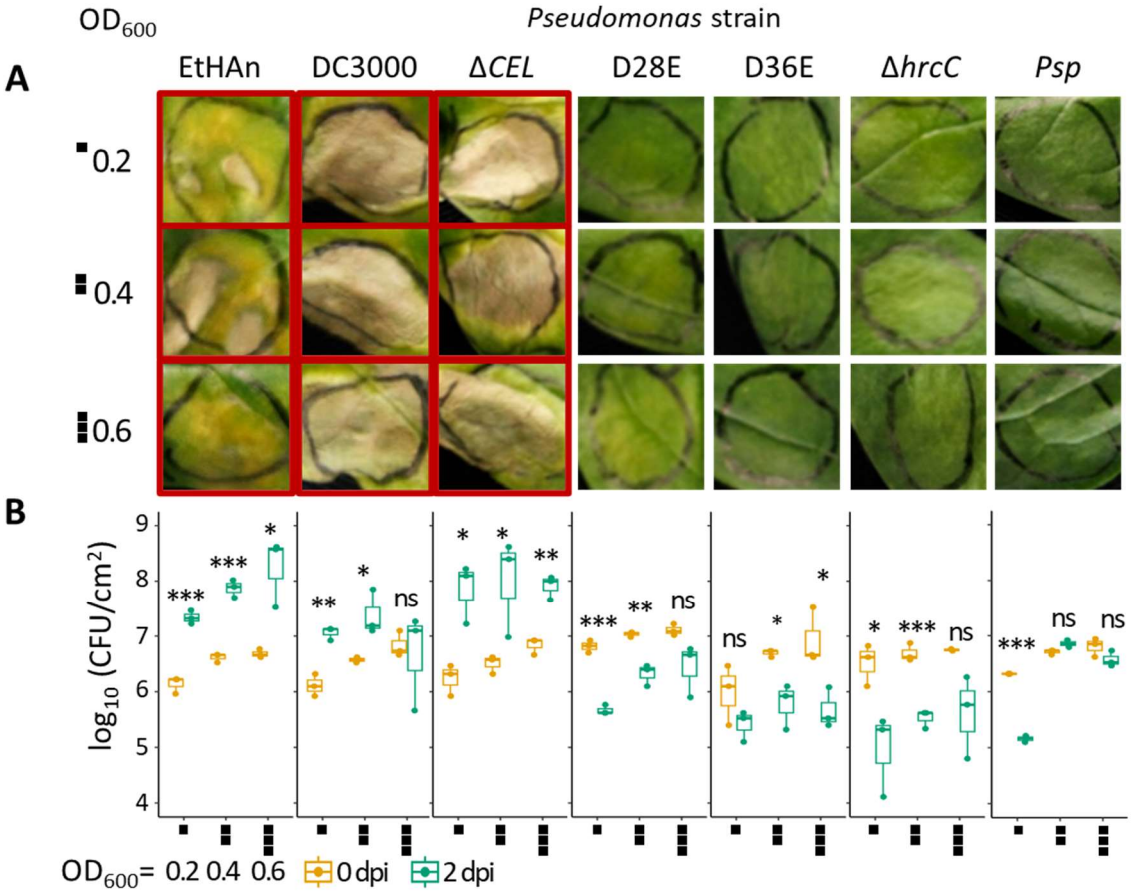

360 **Figure 1: *Pseudomonas syringae* pv. *tomato* DC3000 polymutant D36E is a suitable candidate for**
361 **effector screens in spinach.** We infiltrated seven different *Pseudomonas* strains at OD_{600} equal to 0.2 (1
362 square), equal to 0.4 (two squares), or equal to 0.6 (three squares) into 2.5-3 week old, first true leaves
363 of spinach. **A)** We observed disease symptoms at all tested optical densities in infiltrated spots of the
364 transgenic *Pseudomonas fluorescens* Pf-1 strain EtHAn (EtHAn), the *Pseudomonas syringae* pv. *tomato*
365 strain DC3000 (DC3000), and the DC3000 mutant strain Δ*CEL* (Δ*CEL*). The two DC3000 polymutants D28E
366 (D28E) and D36E (D36E) did not cause strong disease symptoms. The DC3000 T3SS-mutant Δ*hrcC* (Δ*hrcC*)
367 and the bean pathogen *Pseudomonas syringae* pv. *phaseolicola* (*Psp*) did not cause disease symptoms.
368 infiltrated spots were documented 6-7 days post inoculation (dpi). In **B)** We assessed proliferation of the
369 different *Pseudomonas* strains in spinach, by estimating the bacterial titre as colony forming units (CFU)
370 per square centimetre (cm^2). *Pseudomonas* strains leading to visual disease symptoms (EtHAn, DC3000,
371 Δ*CEL*) increased titres between 0 dpi and 2 dpi. Strains without visual disease symptoms, including Δ*hrcC*,
372 *Psp* OD_{600} equal to 0.2 and the polymutants D28E and D36E reduced titres between 0 dpi to 2 dpi.
373 Infiltration of *Psp* at OD_{600} equal to 0.4 or 0.6 stabilised bacterial titres. A Two-tailed t-test was applied
374 to compare 0 dpi and 2 dpi CFU/cm^2 counts (*** $p < 0.001$, ** $p < 0.01$, * $p < 0.05$), n=3 infiltrated spots
375 per treatment and timepoint.

376

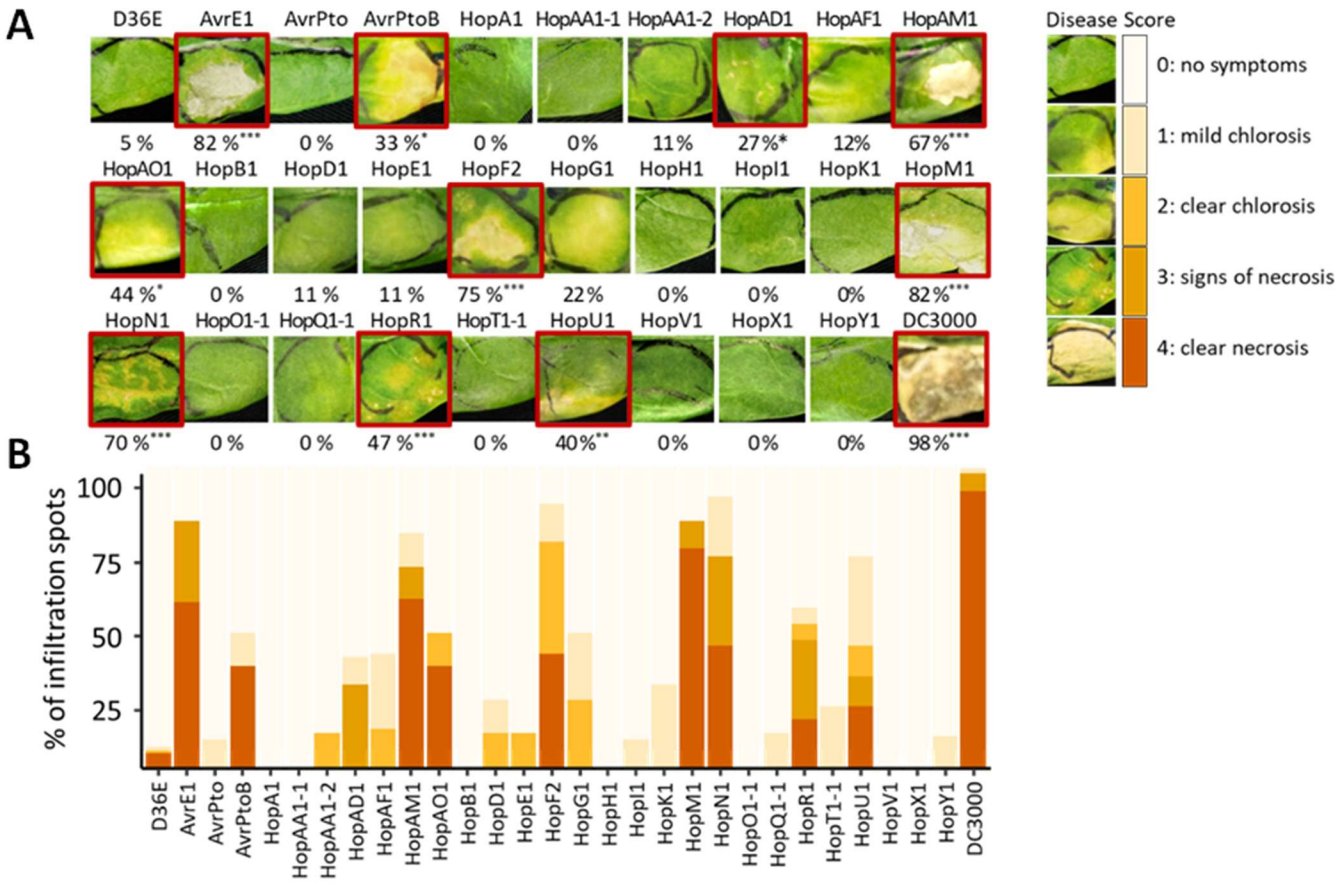

Figure 2: Individual DC3000 effectors in D36E can reconstitute DC3000-like symptoms in spinach. A) Development of disease symptoms after infiltration of D36E, DC3000 and D36E bacteria carrying individual effectors. We scored disease symptoms in each infiltrated spot based on the presented disease score scale ranging from 0 (no symptoms) to 4 (clear necrotic symptoms). Additional disease score scale examples can be found in Figure S2. D36E served as the negative control and induced disease symptoms at a low rate (5 %), while DC3000, equipped with all native effectors and serving as the positive control, caused severe disease symptoms in spinach in the majority of spots (98 %). The percentages depicted below the infiltrated spots indicate the percentage of infiltrated spots developing disease symptoms (score >1). For statistical analysis we applied a Fisher Exact test (*** $p < 0.001$, ** $p < 0.01$, * $p < 0.05$). Effectors affecting the development of disease symptoms significantly ($p < 0.05$) are highlighted with a red frame. **B)** Stacked bar graph summarizing the frequency at which a specific disease score was observed for each effector using the disease score range introduced in A ranging from low (light orange) to high (dark orange). D36E bacteria carrying individual effectors and controls (D36E and DC3000) were infiltrated at OD_{600} equal to 0.4. Development of disease symptoms was assessed at 6-7 dpi, *n*=8-12 infiltrated spots per treatment.

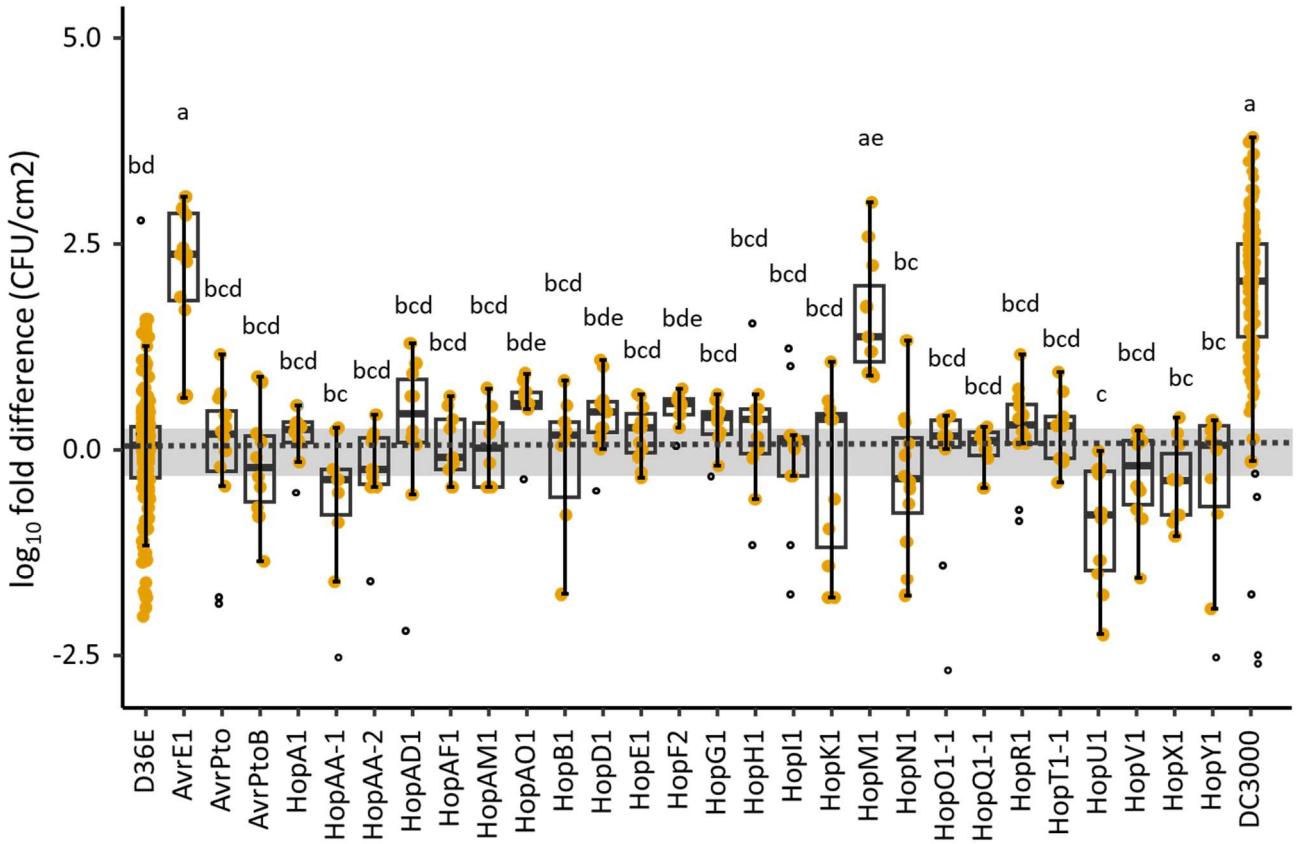

Figure 3: Expression of *AvrE1*, *HopM2*, and *HopU1* significantly alter D36E proliferation and virulence on spinach. We assessed bacterial titres at 2 dpi, as a proxy for bacterial proliferation and ultimately bacterial virulence. D36E without additional effectors served as the negative control and displayed a reduction in titre between 0 dpi and 2 dpi, while DC3000, serving as the positive control, increased titres over this time window (Figure 2, S1). To assess the contribution of individual effectors to D36E proliferation we compared the $\log_{10}$ fold difference between the CFU/cm^2 of D36E carrying an individual effector against the D36E negative control. This revealed that D36E bacteria carrying either *AvrE1* or *HopM1* showed significantly higher titres at 2 dpi, while D36E carrying *HopU1* displayed significantly lower titres. The effectors *HopAO1*, *HopD1* and *HopF2* show a trend towards increasing D36E titres. The effectors *HopAA-1*, *HopN1* and *HopX1* show a trend towards decreasing D36E titres. For statistical analysis we conducted a one-way analysis of variance (ANOVA) followed by a Tukey's Honestly Significant Difference test. The results of the test for significance are indicated by the letters above the boxplots, and *n*=8-12 infiltrated spots per treatment.

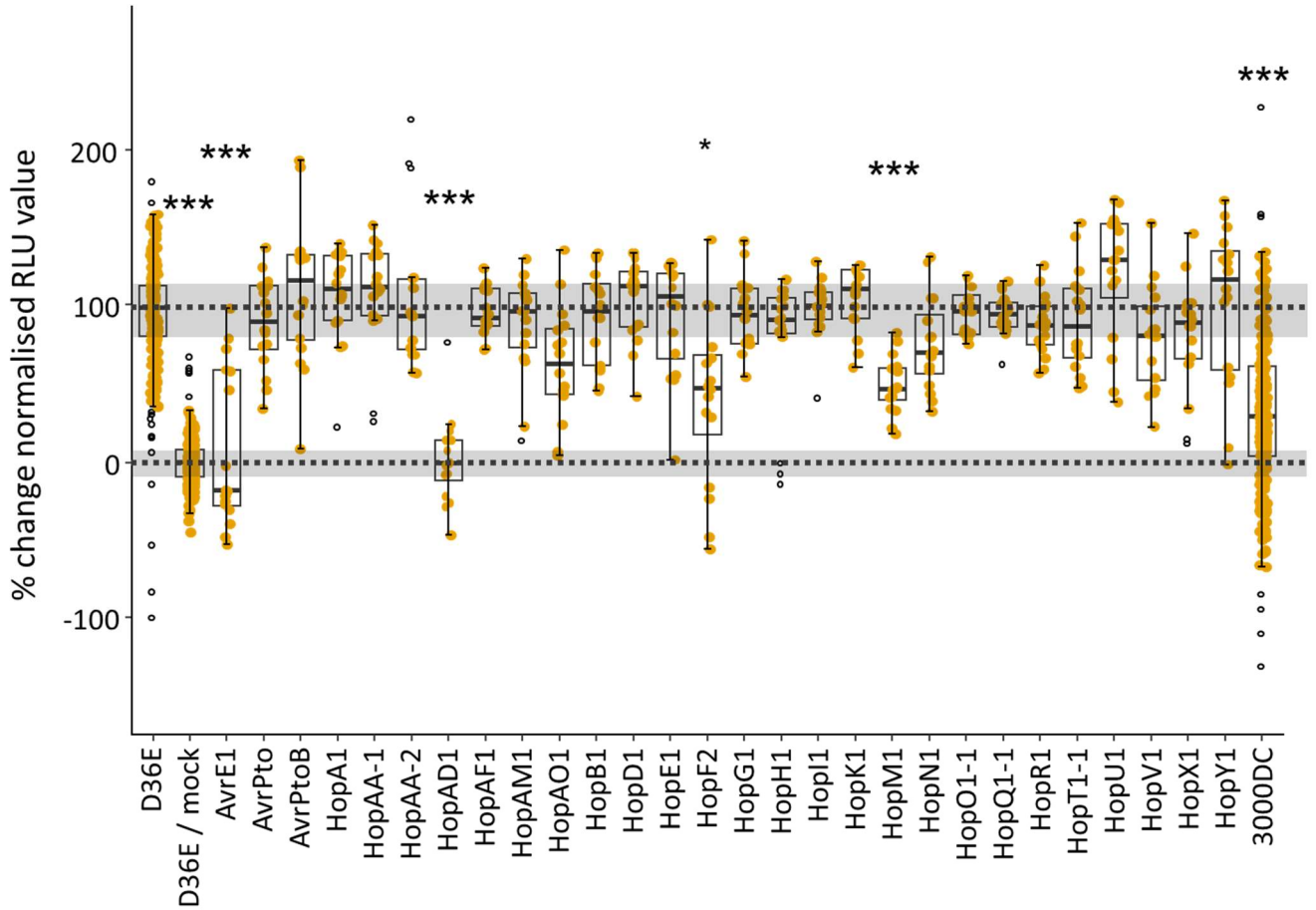

Figure 4: AvrE1, HopAD1, and HopAD1 can act as suppressors of the ROS burst in spinach when delivered by D36E. We analysed the production of reactive oxygen species (ROS) in spinach one day after elicitation with heat-lysed D36E bacterial cells (MAMP-mix/MAMP) (Figure S4). We included ROS burst positive controls (D36E/MAMP) and ROS burst negative control (D36E/MQ, Figure S3). In addition, we included in every batch the effector positive control (DC3000/MAMP) as DC3000 can suppress ROS bursts in a concentration-dependent manner (Figure S5). Infiltration of D36E bacteria carrying *AvrE1*, *HopAD1* and *HopM1* prior to elicitation with the MAMP-mix reduced the ROS burst significantly when compared to D36E. *HopAO1*, *HopF2* and *HopN1* showed a trend towards reducing ROS bursts. Conversely, infiltration with D36E bacteria carrying *HopU1* resulted in an elevated, albeit not significant, production of ROS during the ROS burst. An ANOVA and Dunnett's post-hoc test was applied to compare the normalised and scaled Relative Light Units (RLU) of D36E single effector lines to the median of D36E/MQ controls. Asterisks above the boxplots indicate significant results (*** p=0.001, ** p=0.01, * p=0.05), n=16 leaf discs per treatment.

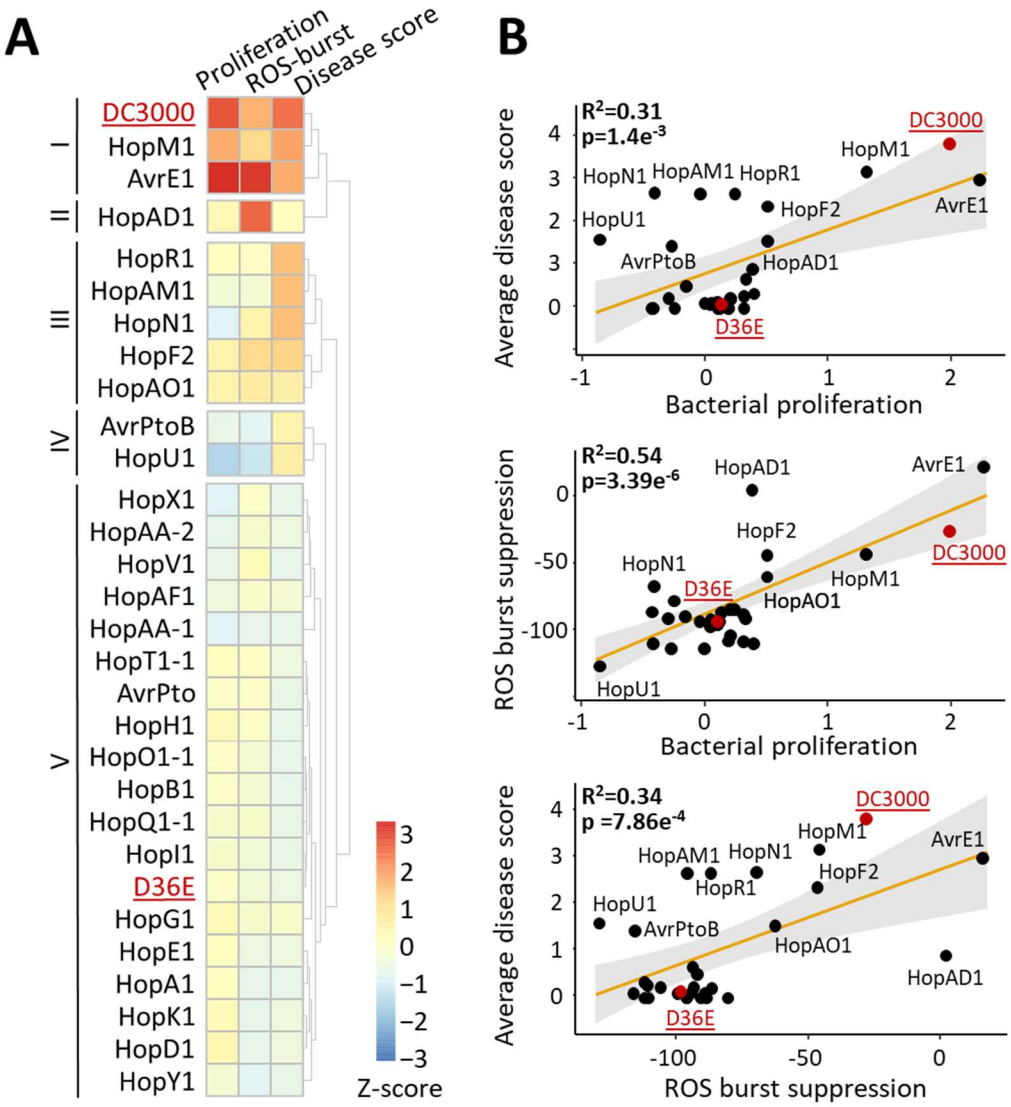

Figure 5: Systematic analysis of the functional effector screens recapitulate the importance of AvrE1 and HopM1 to restore DC3000-like phenotypes on spinach by D36E. To integrate the results of the three effector screens on spinach, we performed a systematic comparison of the phenotypic outcomes. In **A)**, the heatmap depicts the Z-scaled assay read-outs facilitating a comparison of the phenotypic outcomes across the 28 effectors when expressed in D36E. Hierarchical clustering of the Z-scaled values reveal five clusters that differ in their patterns of phenotypic outcomes (cluster I – cluster V). The largest group of 18 DC3000 effectors, depicted as cluster V, did not significantly affect spinach in any of the assays, while *AvrE1* and *HopM1* appear as the most important contributors to DC3000-like symptoms in cluster I. **B)** To better understand the correlation between different assay readouts, we a performed linear regression analysis assessing the prediction of disease scores by proliferation (top), ROS burst suppression by proliferation (middle) and disease scores by ROS burst suppression (bottom). Most effectors cluster together in Cluster V with the negative control D36E as they showed no measurable response (panel A). Consequently, we observe only intermediate R^2 values (0.31-0.54), suggesting that results can only partly be modelled using linear regression. However, the fraction of variation explained

439 by the model is confident, as emphasised by low *p*-values ($3.39e^{-6}$-$1.4e^{-3}$). From the combined analysis,
440 we conclude that effectors which show an impact on disease symptom development, are likely to also
441 impact bacterial virulence and/or the ROS burst. This suggests that disease assays can be used as a proxy
442 for effector pre-selection for further in-depth analysis.

443

444 ## Material and Methods

445 ### Plant material

446 All *in planta* assays were conducted using the spinach cultivar Viroflay (Pop Vriend Seeds, The
447 Netherlands). Seeds were sown and plants were cultivated on Primasta® potting soil within a climate
448 chamber providing a stable environment (21˚C, 16 hr photoperiod, 70% relative humidity,
449 200 µmol m^{2} s^{-1} light intensity). Assays were initiated when the first true leaves were fully expanded,
450 and the second set of true leaves started development, typically occurring between 2.5 and 3 weeks post
451 sowing. To ensure consistency, phenotypically-similar plants were selected for all experiments.

452 ### *Pseudomonas* Infiltration

453 To identify a suitable bacterium for T3SS-dependent effector delivery into spinach, we tested different
454 *Pseudomonas* strains. Preparation of bacterial cultures and infiltration was performed as previously
455 described with the following adaptations (Wei et al., 2013; Liu et al., 2015). Bacteria were grown for two
456 days on King's B (KB) agar medium, supplemented with antibiotics at 28˚C. Antibiotic resistances of the
457 different bacteria are listed in Table S1, and antibiotics concentrations are listed in Table S2. Bacteria
458 were re-streaked to new KB agar plates 2 days prior to infiltration (28˚C). For infiltration, bacteria were
459 scraped off the KB agar plates and suspended in infiltration medium (10 mM $MgSO_4$, 50 µl/l Coatosil
460 1220 surfactant in MilliQ (MQ) water). Bacteria were infiltrated from the abaxial side of fully-expanded
461 spinach leaves with a needleless syringe. Infiltrated spinach plants were placed in trays and covered from
462 the light before transfer to the climate chamber. The cover was removed after one day, exposing the
463 plants to the light conditions. Screening for disease symptom development and bacterial proliferation
464 were performed as described below.

465 ## Generating the D36E single effector library

466 For single effector screens in this study, we obtained the DC3000 single effector library in pENTR/SD/D-
467 TOPO backbones and the matching Gateway destination vector pCPP5372 (Addgene, (Wei et al., 2018).
468 Single *Escherichia coli* colonies were picked and grown in overnight liquid Luria-Bertani (LB) medium
469 supplemented with selective antibiotics (Table S1, S2, S3). Plasmids were isolated using the QIAprep®
470 Spin Miniprep Kit (Qiagen), followed by Sanger sequencing with the M13 forward primers to confirm
471 effector identity (Table S4). We mobilised DC3000 effector genes into *pCPP5372* by Gateway® LR cloning
472 as previously described (Wei et al., 2018). For propagation, plasmids were transformed into Top10 *E. coli*
473 cells and grown on LB agar plates with selective antibiotics (Table S1, S2, S3). We selected positive
474 colonies by colony-check PCR using effector-specific reverse primers and the pCPP5372_pre_attR1
475 forward primer (Table S4). Effector expression plasmids were mobilised from *E. coli* into D36E by
476 triparental mating using the pRK2013 *E. coli* HB101 with the *pRK2013* helper plasmid (Table S1).

477 ## Disease symptom assays

478 To assess the visual development of disease symptoms, *Pseudomonas* strains were prepared and
479 infiltrated as described above. After infiltration, plants were grown until visual assessment of disease
480 symptoms at 6-7 dpi. In order to evaluate the disease symptoms of the single effector library on spinach,
481 we infiltrated each leaf with the negative control D36E and the positive control DC3000, alongside D36E
482 carrying individual effectors. D36E does not trigger disease symptoms while DC3000 does. The two
483 remaining infiltrated spots per leaf were infiltrated with the individual effector lines. We established a
484 disease score ranging from disease score 0 to disease score 4, corresponding to no symptoms (0), mild
485 chlorosis (1), clear chlorosis (2), signs of necrosis (3) and clear necrosis (4) (Figure 2, S2). A Fisher's Exact
486 test was applied to compare incidences of disease symptom-positive infiltrated spots (disease score >1)

487 against the incidence of disease symptom-free infiltrated spots (disease score <2). The number of
488 infiltrated spots showing a specific disease score was plotted using the *R* package *ggplot2* (Wickham,
489 2016; Team;, 2021).

490 D36E proliferation assays

491 To better understand the connection between disease phenotype and virulence of *Pseudomonas* strains,
492 we assessed bacterial proliferation as a proxy for virulence by evaluating bacterial titres. We adapted
493 the published protocol by Liu et al. (2015) (Liu et al., 2015). First, spinach leaves were infiltrated with
494 *Pseudomonas* strains as described above. Then, infiltrated leaves were allowed to dry for 1.5 to 2 hours
495 before collecting 0 dpi samples. These samples were used to verify successful, homogenous infiltration.
496 Three leaf discs (4 mm diameter) per infiltrated spot were collected in 500 µl infiltration medium
497 containing three glass beads (2 mm). Bacterial cells were extracted from spinach tissue by applying tissue
498 lysis using the TissueLyser II (Qiagen, 85300) until leaf discs were completely homogenized (twice 2 min,
499 30 hz s^{-1}). We prepared 10-fold serial dilutions of homogenized samples in infiltration medium using 96-
500 well plates. From all dilution steps, 5-µl droplets were transferred to square KB agar plates with
501 appropriate antibiotics (Table S1, S2). Droplets were allowed to dry and plates were then sealed with
502 Parafilm (Bemis, PM996) and incubated for 1.5 to 2 days at 28°C until colonies were clearly visible.
503 Bacterial titres were estimated by counting colony forming units (CFUs) on KB agar plates. CFUs counts
504 at the highest dilution level with >3 three colonies, were used to calculate the number of CFUs per cm^2
505 spinach leaf.

506 Data were processed in *R* and plotted in *ggplot2* (Wickham, 2016). For statistical analysis of initial
507 *Pseudomonas* screens (Figure 1), we assessed differences in proliferation between 0 dpi and 2 dpi using
508 a two-tailed t-test. For statistical analysis of the single effector library screens at 2 dpi, relative to the

509 D36E negative control, we applied an ANOVA followed by a Tukey post-hoc test. Scripts and raw data
510 are available on GitHub.

511 D36E-compatible ROS burst assays in spinach

512 We modified the ROS burst assay from (Johanndrees et al., 2022), based on (Bisceglia et al., 2015) to
513 make it compatible with the D36E effector delivery system in spinach. First, we identified elicitors for
514 ROS bursts in spinach. Spinach leaf discs (4 mm diameter) were harvested from 2.5-3 week-old plants
515 and washed trice in MQ water (30 min, gentle shaking). Discs were arranged on a 96-well plate (Greiner
516 Bio-One; 655075) in 200 µl MQ water, wrapped in aluminium foil to shield from light, and incubated at
517 21˚C overnight. MQ was replaced with the luminol analogue L-012 sodium salt (Merck SML2236, final
518 concentration 180 µM) and horseradish peroxidase (Merck; P8125-5KU, 0.125 units per reaction)
519 solution. To each sample well, 50 µL elicitor solution was added at concentrations specified in Table S5.
520 We tested chitin, flg22, nlp24 and heat-lysed *Peronospora effusa* race-1 spores (15 min, 100˚C; *Pe1*
521 spores) and heat-lysed D36E cells (15 min, 100˚C; MAMP-mix). Additional details on elicitors can be found
522 in Table S5. Chemiluminescence was measured every 2.5 min in a GloMax® 96 Microplate Luminometer
523 (Promega).

524 To investigate the impact of effectors on the ROS burst in spinach using the D36E effector delivery
525 system, we first established the proper controls. Bacteria were cultivated and infiltrated at 0 dpi as
526 described above. Infiltrated spinach plants were dried for 1.5 to 2 hours before proceeding with the ROS
527 assay protocol as described above. D36E/MQ was established as negative control, D36E/MAMPs as
528 positive control, DC3000/MAMPs as effector-positive control which suppresses ROS bursts (Figure S3,
529 S4, S5). To compare ROS burst assays, $\log_2$ of raw Relative Light Units (RLUs) were calculated and plotted
530 using *ggplot2* in R (Wickham, 2016). Additional features, time to peak ROS scores, peak ROS score and

531 total ROS scores, were calculated using Python 3.10 (van Rossum and Drake, 2009). To screen the
532 complete single effector library for alterations in MAMP-mix elicited ROS bursts, all three controls were
533 included. To analyse the variable results of single effector library screens, we processed, normalised and
534 transformed raw RLUs in Python 3.10 with *pandas* version 1.5 using the internal positive and negative
535 controls for scaling (van Rossum and Drake, 2009; team, 2020). Statistical analysis using ANOVA followed
536 by a Dunnett's post hoc test and visualization was conducted in *R* using *ggplot2* (Wickham, 2016; Team;,
537 2021). All scripts and raw data available on GitHub.

538 Systematic analysis of single effector library screens on spinach

539 We constructed a heatmap using the *pheatmap* package in *R* (Kolde, 2018; Team;, 2021). Phenotypic
540 outcomes are presented by extraction of representative single-values from disease symptom assays,
541 bacterial proliferation assays and ROS burst assays. ROS burst values were inverted by multiplication
542 with -1 to allow for intuitive presentation of effector contribution to disease. We clustered rows using
543 the Euclidean distance metric combined with complete linkage mapping for hierarchical clustering
544 (*pheatmap* default). To facilitate an ordered discussion of the heatmap, we manually rotated the leaves
545 of the dendrogram. Linear regression was conducted by calculating R^2 values using a linear model,
546 corresponding p-values are presented. Results were plotted in *R* using *ggplot2* (Wickham, 2016; Team;,
547 2021). Scripts and raw data are available on GitHub.

Acknowledgments

This project was financially supported by the TopSector TKI Tuinbouw & Uitgangsmaterialen, the Netherlands, and four private spinach breeding companies: Enza Zaden Research & Development B.V. (NL), Pop Vriend Seeds (subsidiary of KWS Vegetables BV) (NL), Rijk Zwaan Breeding B.V. (NL), and Syngenta (NL).

We are grateful for the generosity of the research community in sharing bacterial strains. Special thanks to Alan Collmer, Professor Emeritus of Cornell University, and Wei Zhang, Cornell University, for providing the DC3000 D36E and D28E strains, and to Jeff Chang of Oregon State University for sharing the EtHAn strain.

558 ## References

559 Alfano, J.R., Charkowski, A.O., Deng, W.-L., Badel, J.L., Petnicki-Ocwieja, T., van Dijk, K., and Collmer, A. 2000. The
560 *Pseudomonas syringae* Hrp pathogenicity island has a tripartite mosaic structure composed of a cluster of
561 type III secretion genes bounded by exchangeable effector and conserved effector loci that contribute to
562 parasitic fitness and pathogenicity in plants. Proceedings of the National Academy of Sciences 97:4856-
563 4861.
564 Arnold, D.L., Lovell, H.C., Jackson, R.W., and Mansfield, J.W. 2011. Pseudomonas syringae pv. phaseolicola: from
565 'has bean' to supermodel. Molecular Plant Pathology 12:617-627.
566 Badel, J.L., Shimizu, R., Oh, H.-S., and Collmer, A. 2006. A Pseudomonas syringae pv. tomato avrE1/hopM1 Mutant
567 Is Severely Reduced in Growth and Lesion Formation in Tomato. Molecular Plant-Microbe Interactions
568 19:99-111.
569 Baltrus, D.A., Nishimura, M.T., Romanchuk, A., Chang, J.H., Mukhtar, M.S., Cherkis, K., Roach, J., Grant, S.R., Jones,
570 C.D., and Dangl, J.L. 2011. Dynamic Evolution of Pathogenicity Revealed by Sequencing and Comparative
571 Genomics of 19 Pseudomonas syringae Isolates. PLOS Pathogens 7:e1002132.
572 Bhattarai, G., Yang, W., Shi, A., Feng, C., Dhillon, B., Correll, J.C., and Mou, B. 2021. High resolution mapping and
573 candidate gene identification of downy mildew race 16 resistance in spinach. BMC Genomics 22:478.
574 Bisceglia, N.G., Gravino, M., and Savatin, D.V. 2015. Luminol-based assay for detection of immunity elicitor-
575 induced hydrogen peroxide production in Arabidopsis thaliana leaves. Bio-protocol 5:e1685-e1685.
576 Buell, C.R., Joardar, V., Lindeberg, M., Selengut, J., Paulsen, I.T., Gwinn, M.L., Dodson, R.J., Deboy, R.T., Durkin,
577 A.S., Kolonay, J.F., Madupu, R., Daugherty, S., Brinkac, L., Beanan, M.J., Haft, D.H., Nelson, W.C., Davidsen,
578 T., Zafar, N., Zhou, L., Liu, J., Yuan, Q., Khouri, H., Fedorova, N., Tran, B., Russell, D., Berry, K., Utterback,
579 T., Van Aken, S.E., Feldblyum, T.V., D'Ascenzo, M., Deng, W.-L., Ramos, A.R., Alfano, J.R., Cartinhour, S.,
580 Chatterjee, A.K., Delaney, T.P., Lazarowitz, S.G., Martin, G.B., Schneider, D.J., Tang, X., Bender, C.L., White,
581 O., Fraser, C.M., and Collmer, A. 2003. The complete genome sequence of the *Arabidopsis* and tomato
582 pathogen *Pseudomonas syringae* pv. *tomato* DC3000. Proceedings of the National Academy of Sciences
583 100:10181-10186.
584 Cai, X., Sun, X., Xu, C., Sun, H., Wang, X., Ge, C., Zhang, Z., Wang, Q., Fei, Z., Jiao, C., and Wang, Q. 2021. Genomic
585 analyses provide insights into spinach domestication and the genetic basis of agronomic traits. Nature
586 Communications 12:7246.
587 Chang, J.H., Urbach, J.M., Law, T.F., Arnold, L.W., Hu, A., Gombar, S., Grant, S.R., Ausubel, F.M., and Dangl, J.L.
588 2005. A high-throughput, near-saturating screen for type III effector genes from Pseudomonas syringae.
589 Proceedings of the National Academy of Sciences 102:2549-2554.
590 Cunnac, S., Chakravarthy, S., Kvitko, B.H., Russell, A.B., Martin, G.B., and Collmer, A. 2011. Genetic disassembly
591 and combinatorial reassembly identify a minimal functional repertoire of type III effectors in
592 Pseudomonas syringae. Proceedings of the National Academy of Sciences 108:2975-2980.
593 Deb, D., Mackey, D., Opiyo, S.O., and McDowell, J.M. 2018. Application of alignment-free bioinformatics methods
594 to identify an oomycete protein with structural and functional similarity to the bacterial AvrE effector
595 protein. PLOS ONE 13:e0195559.
596 DebRoy, S., Thilmony, R., Kwack, Y.-B., Nomura, K., and He, S.Y. 2004. A family of conserved bacterial effectors
597 inhibits salicylic acid-mediated basal immunity and promotes disease necrosis in plants. Proceedings of
598 the National Academy of Sciences 101:9927-9932.
599 Ditta, G., Stanfield, S., Corbin, D., and Helinski, D.R. 1980. Broad host range DNA cloning system for gram-negative
600 bacteria: construction of a gene bank of Rhizobium meliloti. Proceedings of the National Academy of
601 Sciences 77:7347-7351.
602 Fabro, G., Steinbrenner, J., Coates, M., Ishaque, N., Baxter, L., Studholme, D.J., Körner, E., Allen, R.L., Piquerez,
603 S.J.M., Rougon-Cardoso, A., Greenshields, D., Lei, R., Badel, J.L., Caillaud, M.-C., Sohn, K.-H., Van den
604 Ackerveken, G., Parker, J.E., Beynon, J., and Jones, J.D.G. 2011. Multiple Candidate Effectors from the

605 Oomycete Pathogen Hyaloperonospora arabidopsidis Suppress Host Plant Immunity. PLOS Pathogens
606 7:e1002348.
607 Fletcher, K., Shin, O.-H., Clark, K.J., Feng, C., Putman, A.I., Correll, J.C., Klosterman, S.J., Van Deynze, A., and
608 Michelmore, R.W. 2022. Ancestral Chromosomes for Family Peronosporaceae Inferred from a Telomere-
609 to-Telomere Genome Assembly of Peronospora effusa. Molecular Plant-Microbe Interactions 35:450-463.
610 Gao, S., Lu, T., She, H., Xu, Z., Zhang, H., Liu, Z., and Qian, W. 2022. Fine Mapping and Identification of a Candidate
611 Gene of Downy Mildew Resistance, RPF2, in Spinach (Spinacia oleracea L.). International Journal of
612 Molecular Sciences 23.
613 Hulse-Kemp, A.M., Bostan, H., Chen, S., Ashrafi, H., Stoffel, K., Sanseverino, W., Li, L., Cheng, S., Schatz, M.C.,
614 Garvin, T., du Toit, L.J., Tseng, E., Chin, J., Iorizzo, M., and Van Deynze, A. 2021. An anchored chromosome-
615 scale genome assembly of spinach improves annotation and reveals extensive gene rearrangements in
616 euasterids. The Plant Genome 14:e20101.
617 Jayaraman, J., Yoon, M., Applegate, E.R., Stroud, E.A., and Templeton, M.D. 2020. AvrE1 and HopR1 from
618 Pseudomonas syringae pv. actinidiae are additively required for full virulence on kiwifruit. Molecular plant
619 pathology 21:1467-1480.
620 Jin, L., Ham, J.H., Hage, R., Zhao, W., Soto-Hernández, J., Lee, S.Y., Paek, S.-M., Kim, M.G., Boone, C., Coplin, D.L.,
621 and Mackey, D. 2016. Direct and Indirect Targeting of PP2A by Conserved Bacterial Type-III Effector
622 Proteins. PLOS Pathogens 12:e1005609.
623 Johanndrees, O., Baggs, E.L., Uhlmann, C., Locci, F., Läßle, H.L., Melkonian, K., Käufer, K., Dongus, J.A., Nakagami,
624 H., Krasileva, K.V., Parker, J.E., and Lapin, D. 2022. Variation in plant Toll/Interleukin-1 receptor domain
625 protein dependence on ENHANCED DISEASE SUSCEPTIBILITY 1. Plant Physiology 191:626-642.
626 Jones, J.D.G., and Dangl, J.L. 2006. The plant immune system. Nature 444:323-329.
627 Jwa, N.S., and Hwang, B.K. 2017. Convergent Evolution of Pathogen Effectors toward Reactive Oxygen Species
628 Signaling Networks in Plants. Frontiers in Plant Science 8:1687.
629 Kandel, S.L., Hulse-Kemp, A.M., Stoffel, K., Koike, S.T., Shi, A., Mou, B., Van Deynze, A., and Klosterman, S.J. 2020.
630 Transcriptional analyses of differential cultivars during resistant and susceptible interactions with
631 Peronospora effusa, the causal agent of spinach downy mildew. Scientific reports 10:6719-6719.
632 Kandel, S.L., Mou, B., Shishkoff, N., Shi, A., Subbarao, K.V., and Klosterman, S.J. 2019. Spinach Downy Mildew:
633 Advances in Our Understanding of the Disease Cycle and Prospects for Disease Management. Plant
634 Disease 103:791-803.
635 Klein, J., Neilen, M., van Verk, M., Dutilh, B.E., and Van den Ackerveken, G. 2020. Genome reconstruction of the
636 non-culturable spinach downy mildew Peronospora effusa by metagenome filtering. PLoS ONE
637 15:e0225808.
638 Kolde, R. (2018). Pretty Heatmaps.
639 Krasileva, K.V., Zheng, C., Leonelli, L., Goritschnig, S., Dahlbeck, D., and Staskawicz, B.J. 2011. Global analysis of
640 Arabidopsis/downy mildew interactions reveals prevalence of incomplete resistance and rapid evolution
641 of pathogen recognition. PLOS ONE 6:e28765.
642 Kvitko, B.H., Park, D.H., Velásquez, A.C., Wei, C.F., Russell, A.B., Martin, G.B., Schneider, D.J., and Collmer, A. 2009.
643 Deletions in the repertoire of Pseudomonas syringae pv. tomato DC3000 type III secretion effector genes
644 reveal functional overlap among effectors. PLoS Pathog 5:e1000388.
645 Liu, X., Sun, Y., Kørner, C.J., Du, X., Vollmer, M.E., and Pajerowska-Mukhtar, K.M. 2015. Bacterial Leaf Infiltration
646 Assay for Fine Characterization of Plant Defense Responses using the Arabidopsis thaliana-Pseudomonas
647 syringae Pathosystem. Journal of Visualized Experiments.
648 Liu, Y., Zeng, Z., Zhang, Y.-M., Li, Q., Jiang, X.-M., Jiang, Z., Tang, J.-H., Chen, D., Wang, Q., Chen, J.-Q., and Shao,
649 Z.-Q. 2021. An angiosperm NLR Atlas reveals that NLR gene reduction is associated with ecological
650 specialization and signal transduction component deletion. Molecular Plant 14:2015-2031.
651 Lozano-Durán, R., Bourdais, G., He, S.Y., and Robatzek, S. 2014. The bacterial effector HopM1 suppresses PAMP-
652 triggered oxidative burst and stomatal immunity. New Phytologist 202:259-269.

653 Lu, X., Kracher, B., Saur, I.M.L., Bauer, S., Ellwood, S.R., Wise, R., Yaeno, T., Maekawa, T., and Schulze-Lefert, P.
654 2016. Allelic barley MLA immune receptors recognize sequence-unrelated avirulence effectors of the
655 powdery mildew pathogen. Proceedings of the National Academy of Sciences 113:E6486-E6495.
656 Mersmann, S., Bourdais, G., Rietz, S., and Robatzek, S. 2010. Ethylene signaling regulates accumulation of the FLS2
657 receptor and is required for the oxidative burst contributing to plant immunity. Plant Physiology 154:391-
658 400.
659 Neilen, M. (2020). RxLR and CRN effectors of the spinach downy mildew Peronospora effusa and their interacting
660 plant proteins. In Plant-Microbe Interactions (Utrecht: Utrecht University).
661 Ngou, B.P.M., Ahn, H.-K., Ding, P., and Jones, J.D.G. 2021. Mutual potentiation of plant immunity by cell-surface
662 and intracellular receptors. Nature 592:110-115.
663 Ngou, B.P.M., Ding, P., and Jones, J.D.G. 2022. Thirty years of resistance: Zig-zag through the plant immune system.
664 The Plant Cell 34:1447-1478.
665 Nomura, K., Andreazza, F., Cheng, J., Dong, K., Zhou, P., and He, S.Y. 2023. Bacterial pathogens deliver water- and
666 solute-permeable channels to plant cells. Nature.
667 Nomura, K., DebRoy, S., Lee, Y.H., Pumplin, N., Jones, J., and He, S.Y. 2006. A bacterial virulence protein suppresses
668 host innate immunity to cause plant disease. Science 313:220-223.
669 Oh, H.S., Kvitko, B.H., Morello, J.E., and Collmer, A. 2007. Pseudomonas syringae lytic transglycosylases
670 coregulated with the type III secretion system contribute to the translocation of effector proteins into
671 plant cells. Journal of Bacteriology 189:8277-8289.
672 Oome, S., Raaymakers, T., Cabral, A., Samwel, S., Böhm, H., Albert, I., Nürnberger, T., and Van den Ackerveken, G.
673 2014. Nep1-like proteins from three kingdoms of life act as a microbe-associated molecular pattern in
674 Arabidopsis. Proceedings of the National Academy of Sciences 111.
675 Pelgrom, A.J.E., Eikelhof, J., Elberse, J., Meisrimler, C.-N., Raedts, R., Klein, J., and Van den Ackerveken, G. 2019.
676 Recognition of lettuce downy mildew effector BLR38 in Lactuca serriola LS102 requires two unlinked loci.
677 Molecular Plant Pathology 20:240-253.
678 R Core Team. 2021. R: A Language and Environment for Statistical Computing (Vienna, Austria: R Foundation for
679 Statistical Computing).
680 Ribera, A., Bai, Y., Wolters, A.-M.A., van Treuren, R., and Kik, C. 2020. A review on the genetic resources,
681 domestication and breeding history of spinach (Spinacia oleracea L.). Euphytica 216:48.
682 Roussin-Léveillée, C., Lajeunesse, G., St-Amand, M., Veerapen, V.P., Silva-Martins, G., Nomura, K., Brassard, S.,
683 Bolaji, A., He, S.Y., and Moffett, P. 2022. Evolutionarily conserved bacterial effectors hijack abscisic acid
684 signaling to induce an aqueous environment in the apoplast. Cell Host Microbe 30:489-501.e484.
685 Rustgi, S., Naveed, S., Windham, J., Zhang, H., and Demirer, G.S. 2022. Plant biomacromolecule delivery methods
686 in the 21st century. Frontiers in Genome Editing 4.
687 Sánchez-Vallet, A., Mesters, J.R., and Thomma, B.P.H.J. 2015. The battle for chitin recognition in plant-microbe
688 interactions. FEMS Microbiology Reviews 39:171-183.
689 Skiadas, P., Klein, J., Quiroz-Monnens, T., Elberse, J., de Jonge, R., Van den Ackerveken, G., and Seidl, M.F. 2022.
690 Sexual reproduction contributes to the evolution of resistance-breaking isolates of the spinach pathogen
691 Peronospora effusa. Environmental Microbiology 24:1622-1637.
692 The pandas development team. 2020. pandas-dev/pandas: Pandas; (Zenodo).
693 Thomas, W.J., Thireault, C.A., Kimbrel, J.A., and Chang, J.H. 2009. Recombineering and stable integration of the
694 Pseudomonas syringae pv. syringae 61 hrp/hrc cluster into the genome of the soil bacterium
695 Pseudomonas fluorescens Pf0-1. The Plant Journal 60:919-928.
696 Upadhyaya, N., Mago, R., Staskawicz, B., Ayliffe, M., Ellis, J., and Dodds, P. 2013. A Bacterial Type III Secretion
697 Assay for Delivery of Fungal Effector Proteins into Wheat. Molecular Plant-Microbe Interactions 27.
698 Üstün, S., Sheikh, A., Gimenez-Ibanez, S., Jones, A., Ntoukakis, V., and Börnke, F. 2016. The Proteasome Acts as a
699 Hub for Plant Immunity and Is Targeted by Pseudomonas Type III Effectors Plant Physiology 172:1941-
700 1958.

701 van Rossum, G., and Drake, F.L. (2009). Python 3 Reference Manual (Scotts Valley, CA: CreateSpace).
702 Wang, Y., Pruitt, R.N., Nürnberger, T., and Wang, Y. 2022. Evasion of plant immunity by microbial pathogens.
703 Nature Reviews Microbiology 20:449-464.
704 Wei, H.L., and Collmer, A. 2018. Defining essential processes in plant pathogenesis with Pseudomonas syringae
705 pv. tomato DC3000 disarmed polymutants and a subset of key type III effectors. Molecular Plant Pathology
706 19:1779-1794.
707 Wei, H.L., Chakravarthy, S., Mathieu, J., Helmann, T.C., Stodghill, P., Swingle, B., Martin, G.B., and Collmer, A. 2015.
708 Pseudomonas syringae pv. tomato DC3000 Type III Secretion Effector Polymutants Reveal an Interplay
709 between HopAD1 and AvrPtoB. Cell Host Microbe 17:752-762.
710 Wei, H.-L., Chakravarthy, S., Worley, J.N., and Collmer, A. 2013. Consequences of flagellin export through the type
711 III secretion system of Pseudomonas syringae reveal a major difference in the innate immune systems of
712 mammals and the model plant Nicotiana benthamiana. Cellular Microbiology 15:601-618.
713 Wei, H.L., Zhang, W., and Collmer, A. 2018. Modular Study of the Type III Effector Repertoire in Pseudomonas
714 syringae pv. tomato DC3000 Reveals a Matrix of Effector Interplay in Pathogenesis. Cell reports 23:1630-
715 1638.
716 Wickham, H. 2016. ggplot2: Elegant Graphics for Data Analysis. Springer-Verlag New York.
717 Xin, X.-F., Nomura, K., Aung, K., Velásquez, A.C., Yao, J., Boutrot, F., Chang, J.H., Zipfel, C., and He, S.Y. 2016.
718 Bacteria establish an aqueous living space in plants crucial for virulence. Nature 539:524-529.
719 Xu, C., Jiao, C., Sun, H., Cai, X., Wang, X., Ge, C., Zheng, Y., Liu, W., Sun, X., Xu, Y., Deng, J., Zhang, Z., Huang, S., Dai,
720 S., Mou, B., Wang, Q., Fei, Z., and Wang, Q. 2017. Draft genome of spinach and transcriptome diversity of
721 120 Spinacia accessions. Nature Communications 8:15275.
722 Yuan, J., and He, S.Y. 1996. The Pseudomonas syringae Hrp regulation and secretion system controls the
723 production and secretion of multiple extracellular proteins. Journal of Bacteriology 178:6399-6402.
724 Yuan, M., Jiang, Z., Bi, G., Nomura, K., Liu, M., Wang, Y., Cai, B., Zhou, J.-M., He, S.Y., and Xin, X.-F. 2021. Pattern-
725 recognition receptors are required for NLR-mediated plant immunity. Nature 592:105-109.
726 Zhang, L., Hua, C., Janocha, D., Fliegmann, J., and Nürnberger, T. 2023a. Plant cell surface immune receptors—
727 Novel insights into function and evolution. Current Opinion in Plant Biology 74:102384.
728 Zhang, Y., Qiu, L., Zhang, Y., Wang, Y., Wang, Q., Fu, C., Dai, S., and Sun, M. 2023b. A high-efficiency Agrobacterium
729 tumefaciens-mediated transient expression system in the leaves of Spinacia oleracea. Plant Methods
730 [Preprint].
731

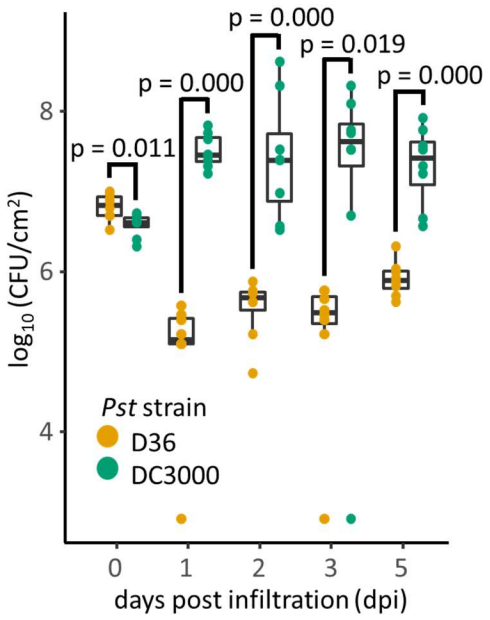

732

733 **Figure S1: DC3000 and D36E titres stabilize at divergent levels over time in spinach.** To evaluate
734 whether bacterial populations stabilise over time, we infiltrated bacterial cultures at 0 dpi at OD_{600} equal
735 to 0.4 and tracked bacterial titres over five days, sampling at 5 time points (0- 3 dpi and 5 dpi). The low
736 variance at 0 dpi is indicative of proper technical reproducibility. Already at 1 dpi it becomes clear that
737 DC3000 cells actively proliferate in spinach while the density of D36E cells drops. Afterwards, both
738 populations appear to stabilize and the difference between titres remains significant and stable until the
739 end of the experiment. For statistical analysis, we applied a two-tailed t-test, with threshold significance
740 level $p < 0.05$.

741

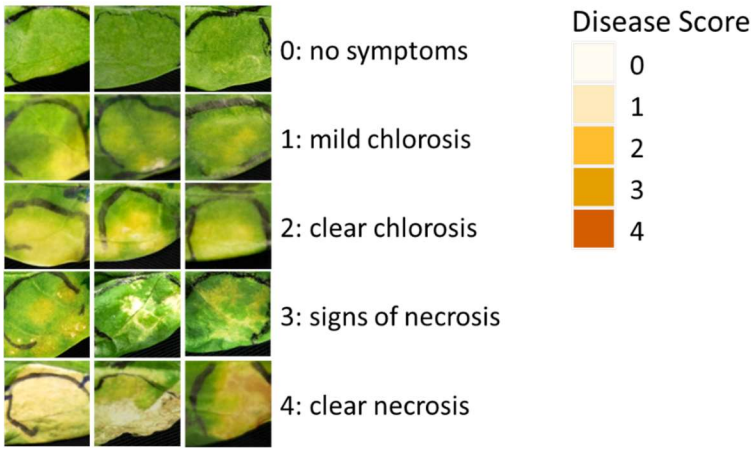

742

743 **Figure S2: Variation in disease symptoms and scoring across the disease score matrix.** We observed
744 substantial variation in disease symptoms on spinach following infiltration with DC3000, D36E and D36E
745 carrying the individual effectors and therefore devised a disease score matrix (Figure 2). The matrix
746 provides a representative overview of the disease symptoms, while also highlighting the variation among
747 the observed disease symptoms.

748

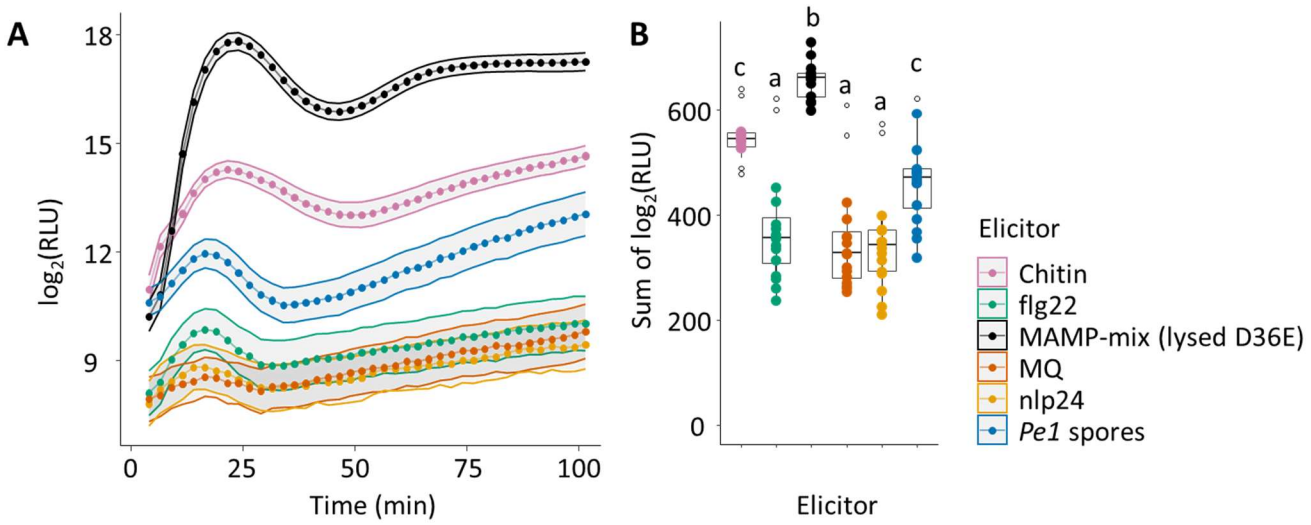

749

750 **Figure S3: Screening putative ROS burst elicitors on spinach.** We tested five different elicitors for their
751 ability to trigger a rapid ROS burst in spinach. We choose the well-described MAMP-type elicitors chitin,
752 flg22 and nlp24, and we included two elicitor mixes, i.e.: heat-lysed D36E (MAMP-mix/MAMP) cells and
753 heat-lysed *Peronospora effusa Race 1* (*Pe1*) spores. We show results as a $\log_2$ transformed raw Relative
754 Light Units (RLUs) values (**A**), and the sum of $\log_2$ transformed raw RLU values over the duration of the
755 experiment (**B**). The MAMP-mix elicited the strongest ROS burst (black), followed by chitin (pink), scoring
756 in sum around 100 $\log_2$(RLU) lower.

757

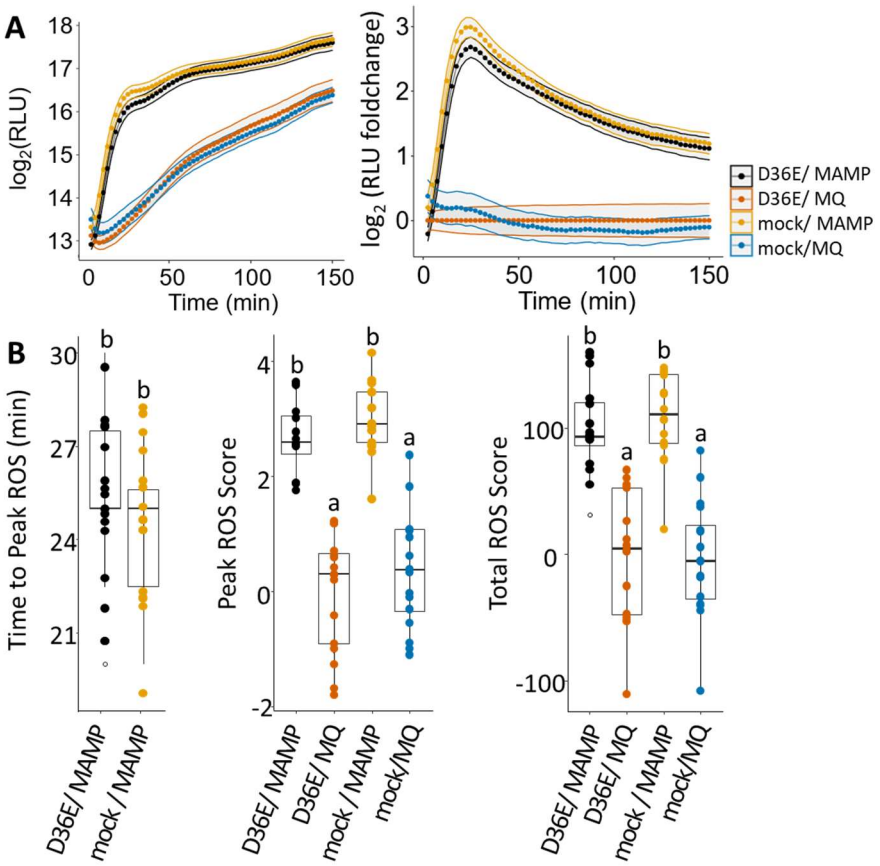

Figure S4: Establishing negative and positive controls for ROS burst assays on spinach in combination with the D36E effector delivery system. A) To establish ROS burst negative and positive controls, we compared mock-infiltrated and non-elicited (mock/MQ) and mock-infiltrated and elicited (mock/MAMP) samples with D36E-infiltrated and non-elicited (D36E/MQ) and D36E-infiltrated and elicited (D36E/MAMP) samples. In both comparisons, D36E had no significant impact on ROS burst results, establishing D36E/MQ as a negative control and D36E/MAMPs as a positive control. For all treatments, we noted a consistent rise in ROS production over time, even in the absence of elicitation (**left**). We normalized our data for this steady increase in background ROS levels by calculating the fold change between the negative control D36E/MQ and measurements of other samples at each timepoint (measurement/control measurement) (**right**). Furthermore, the analysis revealed that no major changes in ROS production are to be expected after ~50 min, which we consequentially used as maximum time during effector screening. **B**) Boxplots display three parameters extracted from the time-resolved graphs depicted in **(A)** after transformation and normalization, i.e.: time to peak ROS (time to maximum ROS production) (**left**), peak ROS scores (maximum of measure ROS scores) (**middle**), and total ROS scores (sum of ROS scores over time) (**right**). Time to peak ROS does not show a statistically significant difference between mock-elicited and MAMP-mix-elicited samples. Peak ROS scores and total ROS scores show significant differences between mock-elicited and elicited samples but no difference between mock-infiltrated and D36E infiltrated samples, confirming the choice of controls for further use. We conducted statistical analysis using ANOVA, followed by Tukey's Honestly Significant Difference test ($p < 0.05$). Distinct letters denote significantly different groups.

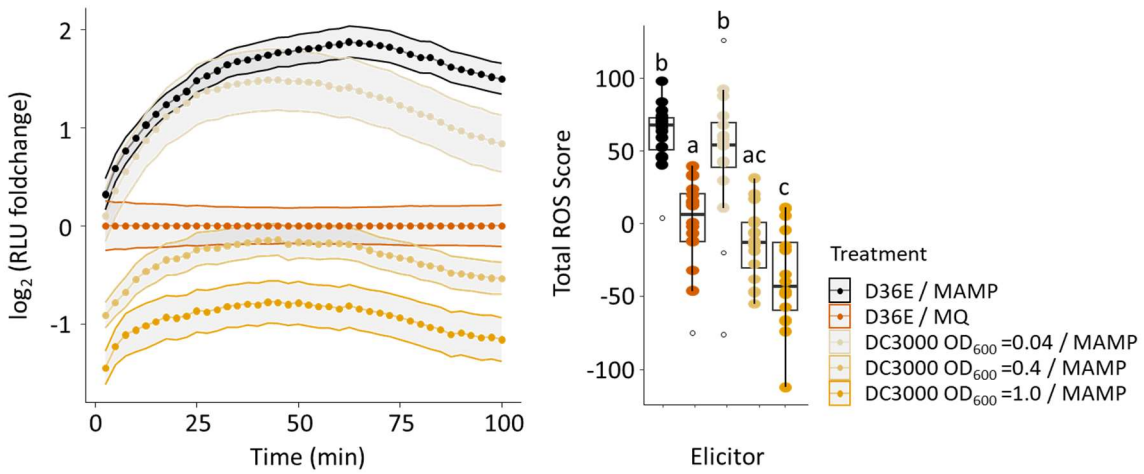

Figure S5: DC3000 supresses ROS bursts in spinach in a concentration-dependent manner. We infiltrated spinach with the ROS burst negative control D36E/MQ, the ROS burst positive control D36E/MAMP or DC3000 at different bacterial densities ranging from OD_{600} equal to 0.04, 0.4, to 1.0 plus the MAMP-mix. We show time-resolved graphs (**left**) and total ROS scores (**right**). Compared to the ROS burst negative control, D36E/MQ, DC3000 OD_{600} equal to 0.04 plus MAMP-mix showed only a trend, but no significant reduction of total ROS scores compared to D36E/MAMP, while DC3000 OD_{600} equal to 0.4 or equal to 1.0 plus MAMP-mix showed total ROS scores significantly lower than D36E/MAMP. Statistical analysis was conducted by ANOVA, followed by a Tukey's Honestly Significant Difference test ($p < 0.05$). Letters above the boxplots indicate statistically significant different groups.

Table S1 Detailed information on the bacterial strains used in this study.

Strain	Description	Resistances	Reference
The Effector-to-Host Analyser (EtHAn)	*Pseudomonas fluorescens* Pf0-1 with the T3SS	Cm^r/Tet^r	(Thomas et al., 2009)
***Pseudomonas syringae pv. tomato* strain DC3000 (DC3000)**	Wildtype, natural pathogen of tomato	Rif^r	(Buell et al., 2003)
D28E	DC3000D28E = CUCPB5585	Rif^r /Sp^r/Ap^r/Sm^r	(Cunnac et al., 2011)
D36E	DC3000D36E = D35EΔ*hopAD1* = CUCPB6119	Rif^r / Sp^r	(Wei et al., 2015)
ΔCEL	DC3000Δ*CEL*	Rif^r / Sp^r	(Alfano et al., 2000)
hrcC	DC3000 *hrcC*$^{--}$ = T3SS$^-$	Rif^r	(Yuan and He, 1996)
***Pseudomonas syringae* pv. *Phaseolicola* (*Psp*)**	Wildtype, natural pathogen of bean	Kan^r	Kind gift of Dr. John W. Mansfield (Arnold et al., 2011)
***E.coli* DH5α**	n/a	n/a	n/a
***E.coli* ccdB survival**	*E. coli* strain used to propagate pCPP5372	n/a	n/a
***E.coli* Top10**	Invitrogen™ One Shot™ TOP10 Chemically Competent *E. coli*	n/a	ThermoFisher Scientific, C404010
E.coli* HB101 *pRK2013		Kan^r	(Ditta et al., 1980)

Table S2: Antibiotics used in this study including abbreviations and standard working concentrations

Antibiotic	Abbreviation	Working concentration (µg/ml)
Ampicillin	Ap	100
Carbenicillin	Cb	100
Chloramphenicol	Cm	10
Gentamycin	Gm	25
Kanamycin	Kan	50
Rifampicin	Rif	50
Spectinomycin	Sp	50
Streptomycin	Stp	50
Tetracycline	Tet	20

Table S3: Plasmids utilized in this study. Including references and plasmid-encoded antibiotic resistances.

Plasmid Name	Resistance	References
pCPP5372	GmR, CmR	(Oh et al., 2007)
DC300 Effector	**pENTR constructs (Wei, 2018)**	**Resistance**
AvrE1	pCPP5912*	Kan^r
AvrPto	pCPP5154	Kan^r
HopA1	pCPP5530	Kan^r
HopB1	pCPP5617	Kan^r
HopD1	pCPP5588	Kan^r
HopE1	pCPP5618	Kan^r
HopF2	pCPP5058*	Kan^r
HopG1	pCPP5238	Kan^r
HopH1	pCPP5306	Kan^r
HopI1	pCPP5571	Kan^r
HopK1	pCPP5099	Kan^r
HopM1	pCPP5233*	Kan^r
HopN1	pCPP5060*	Kan^r
HopO1-1	pCPP5910*	Kan^r
HopQ1-1	pCPP3373	Kan^r
HopR1	pCPP5951	Kan^r
HopT1-1	pCPP3416	Kan^r
HopU1	pCPP5328	Kan^r
HopV1	pCPP5741*	Kan^r
HopX1	pCPP5534	Kan^r
HopY1	pCPP3417	Kan^r
HopAA1-1	pCPP5107	Kan^r
HopAA1-2	pCPP5108	Kan^r
AvrPtoB	pCPP5616	Kan^r
HopAF1	pCPP5539	Kan^r
HopAM1	pCPP5052	Kan^r
HopAO1	pCPP5537	Kan^r
HopAD1	pCPP6450	Kan^r

***** construct includes chaperone

817

Table S4 Primers utilized in this study. All primers were designed specifically for this project 818

Primer target	Direction	Sequence
pCPP5372 pre attR1 site	Fw	CCCTATGACCACTCAAGTGGCG
M13	Fw	CGACGTTGTAAAACGACGGCCAG
5912_Rv	Rev	CTTGGGTGCGCTATGGGTAT
5154_Rv	Rev	CACCCTTTTGCCAGTTACGG
5530_Rv	Rev	AGGCATCGCTGATCACTTCC
5617_Rv	Rev	TCATCGATCACCAGACTGCG
5053_Rv	Rev	GGAGCCCTTCACCATGACAA
5588_Rv	Rev	TTGGACGTGATCTTGGGAGC
5618_Rv	Rev	GGGTCTTGAAGTCCAGCTCC
5058_Rv	Rev	GTAACAGACCCTTTCGACCGG
5238_Rv	Rev	TTTCGCGGAGAGAATGCCTT
5306_Rv	Rev	CGGATGGAGTTCTCTGACGG
5571_Rv	Rev	TCAGGGTGGTTCTTCATCGC
5099_Rv	Rev	CCTTGCAGTAGAGCGTGTCG
5233_Rv	Rev	CAGTTGATCAGCGACCGACT
5060_Rv	Rev	GTATCGCAAGTGAAAGTCTGCTC
5910_Rv	Rev	ACCGCTATTCATTGCCTCGA
MM0038_3373_Rv	Rev	GCGCCCACCCTTATCTGG
MM0039_5951_Rv	Rev	ATGAACAGTGTCGTCTCGGG
MM0040_3416_Rv	Rev	CGCGCCCACCCTTTGAC
MM0041_5328_Rv	Rev	CGCCCACCCTTAATCTGACT
MM0042_5741_Rv	Rev	CCGGATGGCTCTCGAAATGA
MM0043_5534_Rv	Rev	TTTGATGGGCGAGACTTGCT
MM0044_3417_Rv	Rev	CCACCCTTCTGGTAGTTGATGC
MM0045_5107_Rv	Rev	GGATGCAGTCGATTTCACCG
MM0046_5108_Rv	Rev	TCACTTCGAGAAAACGCCGA
MM0047_5616_Rv	Rev	ACATGTCTTTCAAGGGCCGT
MM0048_5539_Rv	Rev	ACCCTTTTGTGCGACCAGAT
MM0049_5052_Rv	Rev	GGTGTGCTTGCCATCATGAC
MM0050_5537_Rv	Rev	TAGTCGTGAAAGGCCTGCAG
MM0051_6450_Rv	Rev	CCCGTGAGTCTTGTCCTAGC

Table S5: Elicitors tested for ROS burst elicitation on spinach.

Elicitor-candidate	Description	Concentration	Producer/ Source	Reference (if applicable)
Chitin	Cell wall component of fungi, recognised by different receptors depending on the plant	4 mg mL^{-1}	Merck C7170, from shrimp shells, processing described in (Johanndrees et al., 2022)	(Sánchez-Vallet et al., 2015)
flg22	22 amino acid peptide of *Pseudomonas aeruginosa* flagellin	0.2 µM	Synthesised by Genscript; RP19986	(Mersmann et al., 2010)
nlp24	24 amino acid peptide of *Hyaloperonospora arabidopsidis* of the necrosis and ethylene-inducing peptide 1-like protein 3 (HaNLP3)	2 µM	Synthesised by Genscript	(Oome et al., 2014)
***Peronospora effusa 1* spores**	Heat-lysed *Peronospora effusa* race 1 spores	150 spores/µL	Spores harvested 14 dpi, cleaned with a vacuum filtration system combining Miracloth, spore collection on a 11 µm Merck Millipore Nylon net filter (NY1104700)	(Klein et al., 2020; Skiadas et al., 2022)
MAMP-mix	Heat-lysed D36E	OD_{600} equal to 1.0	Grown as described above, dilution/re-suspension in MQ	(Wei et al., 2015)

819